Geophys J. R. astr. Soc. (1972) **26**, 427–458

Implications of Heat Flow and Bottom Water Temperature in the Eastern Equatorial Pacific

R. P. Von Herzen and Roger N. Anderson

(Received 1971 July 8)

Summary

The distribution of terrestrial heat flow through the sea floor of the eastern equatorial Pacific Ocean is compared to recent tectonic interpretations of this complex region. Some 500 values between 25° N to 20° S latitude, including 146 newly reported here, show that the theoretical distribution of heat flow for sea-floor spreading models matches well with smoothed data over portions of the Pacific, Cocos and Nasca lithospheric plates created within about the past 18 My from the East Pacific Rise. For the Galapagos Rift Zone, the fit is reasonable for lithosphere formed within the last 5 My only if a significant proportion of low heat-flow values is ignored. The heat flow on the Mathematicians' Ridge and Galapagos Rise indicates that these were sea-floor spreading axes along which activity terminated about 5 and 10 My ago, respectively; this interpretation and its time scale are generally consistent with tectonic histories deduced from magnetic and topographic evidence.

Detailed surveys and repeated measurements at stations suggest that localized heat-flow variability is frequently associated with topographic variability of the sea floor. Bottom water temperature profiles show that the East Pacific Rise is a barrier to eastward flow of waters at depths greater than 3 km, the approximate sill depth over the Nasca plate.

Introduction

Although measurements of heat flow from the Earth's interior were among the first data to support concepts of large-scale dynamic processes (e.g. Bullard, Maxwell & Revelle 1956), the variability in the distribution of values has proved difficult to interpret. Recent global studies have emphasized spherical harmonic analysis (Horai & Simmons 1969) and its correlation with other geophysical data (Horai 1969; Kaula 1966), statistical analyses (Von Herzen & Lee 1969), and deductions from large-scale variations along long profiles in selected regions (Langseth & Von Herzen 1971). Until recently, heat-flow data have not proved as useful for development of specific quantitative tectonic models as, for example, geomagnetism and seismology have been for the tectonics of sea-floor spreading. A statistical analysis of heat-flow data *vs.* age of the crust in the well-surveyed North Pacific has shown, however, a good correlation with theoretical cooling of a lithospheric plate (Sclater & Francheteau 1970). Also, a model incorporating thermal expansion and contraction of lithospheric plates generated at a spreading axis fits well the generalized topography of mid-ocean ridges (Sclater *et al.* 1971a), even if not to individual heat-flow values.

The eastern Pacific Ocean has been a region of intensive investigation of heat-flow

since the measurements of Bullard *et al.* (1956). Including those reported here, there are some 500 values between 25° N and 20° S latitude, from the western coasts of Central and South America to 120° W longitude (Fig. 1). This paper discusses (1) the regional heat-flow and near-bottom water temperature distributions and their relation to plate tectonics, and (2) characteristics of small-scale variability in heat-flow measurements for this region.

Previous work

Physiography and plate tectonics

Menard (1960) first interpreted the gross physiography of the eastern Pacific and approximately mapped the trend of the East Pacific Rise (EPR) from 55° S to the Gulf of California (Fig. 1). Menard (1964) reported the Galapagos fracture zone as an east–west striking fault zone intersecting the EPR at the equator. Herron & Heirtzler (1967) and Raff (1968) found linear magnetic anomalies parallel and symmetrical to the postulated fracture zone, suggesting that it was an active sea-floor

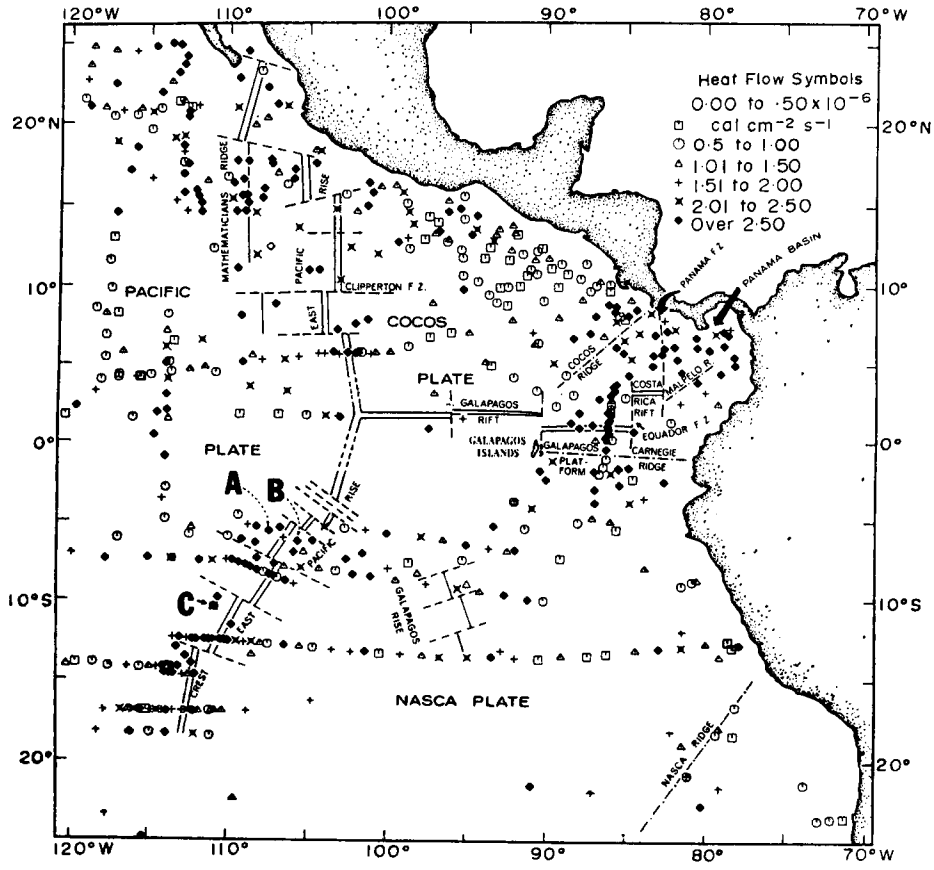

FIG. 1. Physiography and heat-flow measurements of the eastern equatorial Pacific. Heat-flow values are represented by symbols defined in the legend. Double lines represent active spreading ridges, and dashed lines are transform faults. Aseismic ridges are indicated by dash-dot lines, and fossil spreading centres by single solid lines. The Galapagos Ridge and the Costa Rica Rift comprise the Galapagos Rift Zone. A, B, and C represent detailed heat-flow and topographic survey areas.

spreading centre designated the Galapagos Rift Zone (GRZ). Molnar & Sykes (1969) offered seismic evidence for an eastern extension of the GRZ, the Costa Rica Rift.

The major lithospheric plates east of the EPR, the Nasca and Cocos, have been outlined largely on the basis of seismicity by Morgan (1968). Sclater *et al.* (1971a) present evidence that the Mathematicians' Ridge is a fossil ridge crest, and that the EPR has been realigned relatively recently to its present trend. The Galapagos Rise, an aseismic topographic elevation to the east and subparallel to the EPR (Menard, Chase & Smith 1964), is another fossil ridge remaining from that reorganisation of plate boundaries (Herron 1971; Anderson & Sclater 1971). The structure of the Panama basin is only partly deciphered, and its tectonic history remains speculative (van Andel *et al.* 1971). A major unsolved problem is the geological history of four aseismic ridges of the East Pacific, the Cocos, Carnegie, Nasca, and Tehuantepec. The structural complexity of the East Pacific seems to be matched by the complexity of its tectonic development, which is only beginning to be understood.

Heat flow. The heat-flow pattern is obviously complex (Fig. 1), although there are some systematic features of the geographic distribution. These include: (1) High heat flow associated with the topographic crests of spreading ridges. The high values first recognized on the EPR crest (Bullard *et al.* 1956; Von Herzen 1959) and the GRZ crest (McKenzie & Sclater 1969) are the most obvious in the distribution of the East Pacific Ocean heat flux. (2) High values over certain anomalous regions, such as the Panama basin, probably reflect complex and recent tectonic activity, although the nature of the tectonism remains obscure (van Andel *et al.* 1971; Anderson 1971). Another region between 15-20° N latitude *west* of the EPR crest is associated with the Mathematicians' Ridge, which has been interpreted as a fossil spreading centre (Sclater *et al.* 1971a). It appears that a similar explanation is most likely for the moderately high values over the Galapagos Rise, the characteristics of which are detailed below. (3) Low heat flow over relatively large regions near the equator both east and west of the EPR were first outlined by Von Herzen & Uyeda (1963), and detailed studies have particularly confirmed the low associated with the Guatemala basin (Vacquier *et al.* 1967). The additional measurements reported here are not within these features, and no other large areas of low heat flow have been found in the region of this study. (4) Locally variable heat-flow values on the EPR and its flanks were first studied over long profiles across the EPR crest (Von Herzen & Uyeda 1963). We have extended these studies with both profiles and small detailed areal studies, as discussed below.

Techniques and new measurements

The 146 new measurements obtained at 97 localities reported in this paper were carried out on two separate research cruises, Expedition AMPHITRITE of Scripps Institution of Oceanography (Dec. 1963–Feb. 1964), and ATLANTIS II Cruise 54 of Woods Hole Oceanographic Institution (Nov.–Dec. 1969) (Tables 1 and 2). The general principles and design of instrumentation were similar on both cruises, utilizing a probe with multiple temperature sensors lowered from the surface vessel to measure vertical temperature gradients in the sea floor, and a heated needle probe technique to measure thermal conductivity of the recovered sediment cores (Von Herzen & Maxwell 1959). Temperature gradient instrumentation was similar on both cruises, utilizing either a piston-coring apparatus with outrigged thermistor probes mounted to the core barrel (Langseth 1965), or a shorter (2–3 m) probe with outrigged probes attached. The thermistor probes have thermal time-constants of only a few seconds, and both types of apparatus usually required only a few minutes to reach temperature equilibrium with the sediments after penetrating the sea floor. The shorter probes were utilized in studies of local variability by multiple penetrations at the same station or locality.

Table 1

Heat-flow measurements of AMPHITRITE Expedition

Station No.	Lat.	Long.	Depth (m)	Length* Penet. (m)	No. Probes	Therm.‡ Cond.	Heat§ Flow
AMPH-2	19° 25′ N	123° 42′ W	4430	6·1	3	1·98	1·05
AMPH-3	15 02 N	125 09 W	4460	6·1	3	1·89	1·52
AMPH-6	4 51 N	128 22 W	4460	4·5	2	2·06	1·33
AMPH-8	0 31 S	130 09 W	4525	6·0	3	1·98	0·77
AMPH-9	2 05 S	128 21 W	4615	1·4	1	(2·00)	0·4
AMPH-10	4 21 S	125 31 W	4300	6·1	3	2·15	0·86
AMPH-11	6 19 S	123 20 W	4590	1·8	2	(2·00)	0·88
AMPH-12B	7 31 S	121 57 W	4410	6·4	3	1·59	0·62
AMPH-13	7 30 S	117 44 W	4260	6·1	2	2·04	3·86
AMPH-14	7 25 S	115 03 W	4040	1·9	2	(2·07)	2·94
AMPH-15A	7 28 S	113 32 W	3615	1·9	2	2·09	2·86
AMPH-15B	7 28 S	113 35 W	3895	6·1	2	2·09	2·42
AMPH-16	7 35 S	111 49 W	3475	1·4–1·8	2	(2·00)	2·24–2·88
AMPH-17	7 36 S	111 00 W	3470	2·0	2	1·94	2·31
AMPH-18	7 32 S	110 07 W	3395	1·8	2	1·94	1·98
AMPH-19	7 33 S	109 46 W	3315	1·9	2	1·79	2·63
AMPH-20	7 43 S	109 21 W	3300	6·3	3	2·16	3·24
AMPH-21	7 51 S	108 56 W	3240	2·0	2	1·90	2·93
AMPH-22	7 59 S	108 38 W	3200	1·9	2	1·92	6·28
AMPH-23	8 11 S	108 12 W	3045	2·0	2	1·97	7·16
AMPH-24	8 19 S	107 48 W	3090	1·9	2	1·91	0·86
AMPH-25B	8 27 S	107 27 W	3120	2·4	2	2·15	6·71
AMPH-26	8 33 S	107 13 W	3240	2·3	2	2·16	5·20
AMPH-27	8 40 S	106 57 W	3310	2·1	2	2·19	0·75
AMPH-28	8 51 S	106 26 W	3370	2·0	2	2·16	3·44
AMPH-29	9 03 S	105 54 W	3660	1·8	2	2·18	1·77
AMPH-30	10 31 S	110 53 W	3160	2·1	2	1·89	2·40
AMPH-31	10 31 S	110 51 W	3090	6·0	3†	1·98	>7·29†
AMPH-32	10 32 S	110 56 W	3360	2·1	2	1·89	1·29
AMPH-33	10 28 S	110 55 W	3205	2·2	2	1·92	2·74
AMPH-34	18 32 S	111 10 W	3435	6·4	3	2·40	0·99
AMPH-35	18 28 S	112 11 W	3165	2·2	2	2·38	2·28
AMPH-36	18 24 S	113 57 W	3075	2·4	2	1·81	4·70
AMPH-38	18 21 S	116 13 W	3285	1·9	2	2·37	1·37
AMPH-39	18 21 S	116 10 W	3160	2·2	2	2·34	3·44
AMPH-40	18 16 S	118 19 W	3550	6·4	3	2·52	1·92
AMPH-41	18 16 S	121 04 W	3725	6·1	3	2·44	1·32¶
AMPH-42	18 31 S	124 31 W	3865	3·2	2	2·51	3·14
AMPH-43	18 35 S	126 28 W	4030	4·6	3	2·02	1·04
AMPH-44	18 34 S	126 27 W	4030	(1·0)	1	1·75	0·5
AMPH-45	18 31 S	126 28 W	3970	1·5	1	1·75	0·5
AMPH-46	18 32 S	126 33 W	4070	1·8	2	1·76	0·56
AMPH-47A	18 33 S	129 56 W	4180	4·8	3	1·83	1·34
AMPH-48A	18 40 S	133 07 W	3935	2·6	2	1·96	1·22¶
AMPH-48B	18 40 S	133 07 W	3965	1·8	2	2·35	0·94¶
AMPH-50A	18 05 S	145 41 W	4245	(1·5)	1	1·76	1·5
AMPH-51A	17 51 S	147 11 W	4295	2·2	2	2·02	1·03
AMPH-54B	11 28 S	159 38 W	5300	1·8	2	1·73	0·96
AMPH-55	7 30 S	157 40 W	5450	3·4	2	1·75	1·80
AMPH-56	6 04 S	157 28 W	5175	4·3	2	1·65	1·68
AMPH-61	0 25 N	138 10 W	4330	1·8	2	2·13	0·47

* Estimated on basis of gradient, core length, and/or mud smear on barrel or probe. Values in parentheses determined from bend in probe.

† Only one thermistor recorded on scale.

‡ Thermal conductivity values in m cal $°C^{-1}$ cm^{-1} s^{-1}. Values in parentheses assumed from those at nearby stations.

§ Heat flow values in 10^{-6} cal cm^{-2} s^{-1}. Values given to only one figure beyond the decimal point are considered less accurate due to estimated depth of penetration of one thermistor probe.

¶ Upper thermistor registered lower temperature in sediment than in water above bottom.

Table 2

Heat-flow measurements of ATLANTIS II Cruise 54

Station	Latitude	Longitude (W)	Water depth (m)	T	P	N	K	Q	Mean Q
1	4° 53·1′ N	83° 25·9′	3395	2·07	8·9	4	1·72	3·67±0·25	
3	4 52·0 S	87 10·0	3705	1·80	11·7	5	1·83	1·39±0·15	
5	7 24·6 S	89 10·1	4090	1·80	7·4	3	1·57	0·39±0·06	
7	10 00·0 S	91 12·0	4115	1·81	4·4	2	2·68	5·15±0·19*	
8 (1)	9 42·1 S	92 40·1	3975	1·88	2·5	3	(2·51)	3·09±0·29	
(2)	9 42·1 S	92 40·1	3975	1·88	2·0	2	(2·47)	6·08±0·99*	
(3)	9 42·1 S	92 40·1	3975	1·88	2·5	3	(2·51)	5·10±0·42	4·76±0·88
9	9 31·3 S	94 12·6	3745	1·81	8·7	5	2·26	1·24±0·10	
10 (1)	9 19·0 S	95 36·0	3650	1·81	2·5	3	(1·90)	1·83±0·22	
(2)	9 19·0 S	95 36·0	3650	1·81	2·5	3	(1·90)	2·03±0·33	
(3)	9 19·0 S	95 36·0	3650	1·81	1·2	2	(1·83)	2·23±0·70*	2·03±0·12
11 (1)	9 01·9 S	97 36·2	4085	1·85	2·5	3	1·53	1·54±0·23	
(2)	9 01·9 S	97 36·2	4075	1·85	2·5	3	1·53	1·52±0·14	
(3)	9 01·9 S	97 36·2	4070	1·85	2·5	3	1·53	1·51±0·16	1·52±0·01
12	8 49·0 S	99 30·0	4375	1·89	7·7	5	1·76	1·31±0·12	
13 (1)	8 32·7 S	101 06·9	4350	1·89	2·5	3	(1·74)	1·49±0·11	
(2)	8 32·7 S	101 06·9	4350	1·89	2·5	3	(1·74)	2·38±0·12	
(3)	8 32·7 S	101 06·9	4350	1·89	1·2	2	(1·74)	5·74±0·28	3·20±1·29
14 (1)	8 22·2 S	102 13·7	3895	1·80	1·0	1	1·66	4·03±0·41	
15 (1)	8 14·0 S	103 16·0	3875	1·77	2·5	3	(1·82)	0·91±0·04	
16	8 07·0 S	104 19·0	3580	1·76	4·6	3	1·98	1·80±0·10	
17 (1)	8 02·0 S	105° 27·0	3550	1·76	2·5	3	(2·14)	2·68±0·20	
(2)	8 02·0 S	105 27·0	3545	1·76	2·5	3	(2·14)	1·96±0·11	
(3)	8 02·0 S	105 27·0	3545	1·76	2·5	3	(2·14)	2·23±0·14	
(4)	8 02·0 S	105 27·0	3545	1·76	2·5	3	(2·14)	2·18±0·12	
(5)	8 02·0 S	105° 27·0	3480	1·76	2·5	3	(2·14)	1·95±0·10	
(6)	8 02·0 S	105 27·0	3440	1·76	2·5	3	(2·14)	1·82±0·10	2·14±0·13
18	7 58·5 S	106 32·5	3405	1·76	8·1	5	2·39	1·46±0·12	
19 (1)	7 47·0 S	107 08·0	3215	1·76	1·5	2	(2·15)	3·22±0·14*	
(2)	7 47·0 S	107 08·0	3215	1·76	1·5	2	(2·15)	2·88±0·14*	
(3)	7 47·0 S	107 08·0	3215	1·76	2·5	3	(2·18)	2·72±0·22	
(4)	7 47·0 S	107 08·0	3215	1·76	2·5	3	(2·18)	2·94±0·14	2·94±0·10
20 (1)	7 26·0 S	108 15·0	3170	1·73	2·5	3	(1·92)	8·50±0·24	
(2)	7 26·0 S	108 15·0	3170	1·73	2·5	3	(1·92)	7·83±0·30	
(4)	7 26·0 S	108 15·0	3170	1·73	2·5	3	(1·92)	3·62±0·11	
(5)	7 26·0 S	108 15·0	3170	1·73	2·5	3	(1·92)	4·76±0·15	
(6)	7 26·0 S	108 15·0	3170	1·73	2·5	3	(1·92)	3·66±0·14	
(7)	7 26·0 S	108 15·0	3170	1·73	2·5	3	(1·92)	1·57±0·05	
(8)	7 26·0 S	108 15·0	3170	1·73	2·5	3	(1·92)	0·95±0·04	4·41±1·08
22 (1)	5 18·0 S	108 51·0	3470	1·62	2·5	2	1·96	1·73±0·12*	
(2)	5 18·0 S	108 51·0	3470	1·62	2·5	2	1·96	1·78±0·12*	
(3)	5 18·0 S	108 51·0	3470	1·62	2·5	2	1·96	1·71±0·28*	1·74±0·02
24	5 26·0 S	108 15·1	3660	1·63	8·6	5	1·96	4·33±0·22*	
25	5 44·1 S	107 27·2	3255	1·68	6·8	5	1·93	7·20±0·30*	
26 (1)	5 44·8 S	107 29·2	3145	1·69	2·5	3	(1·91)	7·49±0·24	
(2)	5 44·8 S	107 29·2	3145	1·69	2·5	3	(1·91)	7·79±0·25	7·64±0·15
27 (1)	5 43·3 S	107 27·0	3220	1·69	2·5	3	(1·91)	7·45±0·25	
(2)	5 43·3 S	107 27·0	3220	1·69	2·5	3	(1·91)	7·95±0·26	7·70±0·25
28 (1)	5 39·5 S	107 32·7	3195	1·68	2·5	3	(1·95)	6·09±0·29	
(2)	5 39·7 S	107 32·8	3195	1·68	2·5	3	(1·95)	5·77±0·33	5·93±0·16
29	5 43·8 S	107 34·0	3190	1·66	6·2	4	2·00	7·19±0·47	
30 (1)	6 08·6 S	106 33·7	3020	1·78	2·5	3	(2·10)	1·14±0·06	
(2)	6 08·6 S	106 33·7	3005	1·78	2·8	3	(2·10)	1·74±0·08	
(3)	6 08·6 S	106 33·7	2990	1·78	2·7	3	(2·10)	1·71±0·08	
(4)	6 08·6 S	106 33·7	2985	1·78	2·7	3	(2·10)	2·20±0·10	
(5)	6 08·6 S	106 33·7	3000	1·78	2·7	3	(2·10)	1·94±0·09	1·75±0·17

Table 2—*continued*

Station	Latitude	Longitude (W)	Water depth (m)	T	P	N	K	Q	Mean Q
31	6 24·2 S	105 47·4	3425	1·73	10·4	5	2·29	0·64±0·06	
32 (1)	6 24·4 S	105 40·3	3425	1·75	2·5	3	(2·23)	3·87±0·24	
(2)	6 24·4 S	105 40·3	3430	1·75	2·5	3	(2·23)	4·04±0·25	
(3)	6 24·4 S	105 40·3	3430	1·75	2·5	3	(2·23)	3·97±0·25	3·96±0·05
33 (1)	6 22·9 S	105 44·9	3400	1·75	2·7	3	(2·23)	0·87±0·06	
(2)	6 22·6 S	105 44·8	3400	1·75	3·0	3	(2·23)	0·80±0·07	0·84±0·04
34 (1)	6 23·4 S	105 43·4	3405	1·74	2·5	3	(2·22)	2·52±0·13	
(2)	6 23·4 S	105 43·4	3405	1·74	2·5	3	(2·22)	2·47±0·14	
(3)	6 23·4 S	105 43·4	3405	1·74	2·5	3	(2·22)	2·32±0·12	
(4)	6 23·4 S	105 43·4	3405	1·74	2·5	3	(2·22)	2·23±0·12	2·39±0·07
35	6 18·5 S	105 40·8	3360	1·72	10·3	5	2·27	4·06±0·14*	
36 (1)	5 27·5 S	103 59·9	3585	1·74	2·5	3	(1·96)	2·03±0·20	
(2)	5 27·5 S	103 59·9	3585	1·74	1·5	2	(1·90)	2·95±0·88*	
(4)	5 27·5 S	103 59·9	3555	1·74	2·0	2	(1·90)	⩾1·52*	2·17±0·42
37	5 30·0 S	102 42·0	3835	1·70	8·8	4	1·76	0·67±0·08	
39	5 38·0 S	101 25·3	3755	1·67	10·3	4	2·07	1·69±0·18	
40	5 52·0 S	100 05·0	3820	1·79	1·3	2	(2·10)	4·86±0·56	
44 (1)	6 02·0 S	97 54·0	3725	1·80	2·1	3	(1·86)	2·87±0·44	
(2)	6 02·0 S	97 54·0	3745	1·80	2·1	3	1·86	⩾2·13	2·50±0·37
45	6 16·0 S	96 32·0	3785	1·81	8·9	4	1·83	1·03±0·10	
46	6 33·0 S	95 05·0	3850	1·83	1·5	2	(1·64)	3·12±0·12*	
47	6 46·9 S	93 40·5	3985	1·82	9·6	5	1·64	1·91±0·09	
48 (1)	6 58·5 S	92 30·5	4165	(1·90)	2·5	3	(1·62)	1·04±0·32*	
49 (1)	6 55·0 S	92 01·0	4060	1·84	2·5	3	(1·58)	2·83±0·14*	
(2)	6 55·0 S	92 01·0	4045	1·84	2·5	3	(1·58)	3·26±0·17*	
(3)	6 55·0 S	92 01·0	4045	1·84	2·5	3	(1·60)	3·22±0·21	
(4)	6 55·0 S	92 01·0	4050	1·84	2·5	3	(1·60)	2·40±0·15	2·93±0·26
50	5 32·5 S	91 24·3	4075	1·83	11·8	5	(1·60)	0·99±0·06*	
51 (1)	4 13·0 S	90 57·0	3885	1·83	2·5	3	(1·78)	2·25±0·08	
(2)	4 13·0 S	90 57·0	3900	1·83	2·5	3	(1·78)	2·44±0·10	
(3)	4 13·0 S	90 57·0	3885	1·83	2·5	3	(1·78)	2·61±0·09	
(4)	4 13·0 S	90 57·0	3870	1·83	2·5	3	(1·78)	2·25±0·08	2·39±0·09
52	2 23·5 S	90 05·2	3230	1·79	10·6	4	1·97	2·86±0·14	
53	2 45·0 N	86 46·0	2800	2·05	10·4	5	2·06	3·70±0·36	
54 (1)	3 31·7 N	85 52·6	2930	2·06	2·5	3	(1·89)	4·20±0·13	
(2)	3 31·7 N	85 52·6	2925	2·06	2·5	3	(1·89)	4·24±0·13	
(3)	3 31·7 N	85 52·6	2925	2·06	2·0	3	(1·89)	3·92±0·34	4·12±0·10
55	4 16·2 N	84 05·4	3225	2·06	8·7	4	1·93	4·42±0·59	
56	6 00·2 N	82 43·4	3835	2·11	1·5	2	(1·90)	3·98±0·23*	

NOTES: Water depths corrected for sound velocity by Matthews (1939) tables.

T is bottom water temperature (°C).

P is sediment penetration (m) of lowermost probe used for temperature gradient measurements.

N is number of thermistor probes used for sediment temperature gradient measurements.

K is thermal conductivity (reciprocal of mean thermal resistivity), in m cal $°C^{-1}$ cm^{-1} s^{-1}. Parentheses indicate values assumed from nearby stations.

Q is heat flow with probable errors, in 10^{-6} cal cm^{-2} s^{-1}, computed according to methods in Appendix I.
Mean Q is average of heat flow ± standard error for short probe stations with multiple penetrations.

* Q computed from interval values, as indicated in Appendix I.

The details of the instrumentation for both cruises and the methods of data reduction for AII-54 cruise, are described in Appendices I and II, respectively.

Discussion

Physiography, tectonics and heat flow

Galapagos Rift Zone. The Galapagos Rift Zone (GRZ) is an active sea-floor spreading system characterized by a deep (5000 m) central rift valley bounded by well-developed ridge flanks at its western extreme (Deffeys *et al.* 1971) and only a small topographic bulge at its eastern extreme. It terminates on the west at a triple-junction with two segments of the East Pacific Rise. To the east, the crest is offset 220 km to the north along the Ecuador Fracture Zone, with the rift continuing for 250 km as the east–west striking Costa Rica Rift, terminating at the Panama Fracture Zone. The Galapagos Islands at the western extremity of the Galapagos platform comprise a major topographic feature, located near or within an extension of a fracture zone of the GRZ.

Magnetic anomalies. AII-54 magnetic crossings of the Costa Rica Rift and the Galapagos Rift correlate well with tracks reported in Herron & Heirtzler (1967) and Grim (1970) (Fig. 2). We calculate spreading rates of 3·1 cm/yr for both ridge segments. (Spreading rates given in this paper will refer to the velocity of one side of the plate motion with respect to the spreading axis, or half of the velocity between symmetrically spreading plates.) Anomaly 3 (5 My) is the oldest identified here. Herron (1971) has identified anomaly 5 (10 My) on the Costa Rica Rift, but it has not been found west of the Galapagos Islands.

Amplitudes of magnetic anomaly profiles across the two ridge segments of the Ecuador Fracture Zone are significantly different: ±500 gammas on the Galapagos Rift and ±250 gammas on the Costa Rica Rift (Fig. 3). The following explanations seem possible, although our relatively meagre data do not allow a preference of interpretation:

(1) The remanent magnetization and/or thickness of the magnetized layer may be different across the two ridge segments. If so, differences in petrology or processes of

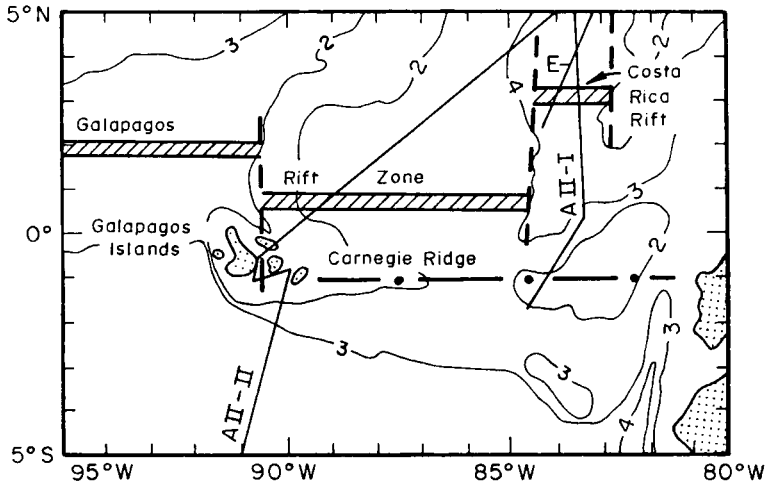

FIG. 2. Index map of AII-54 cruise magnetic profiles across the Galapagos Rift Zone.

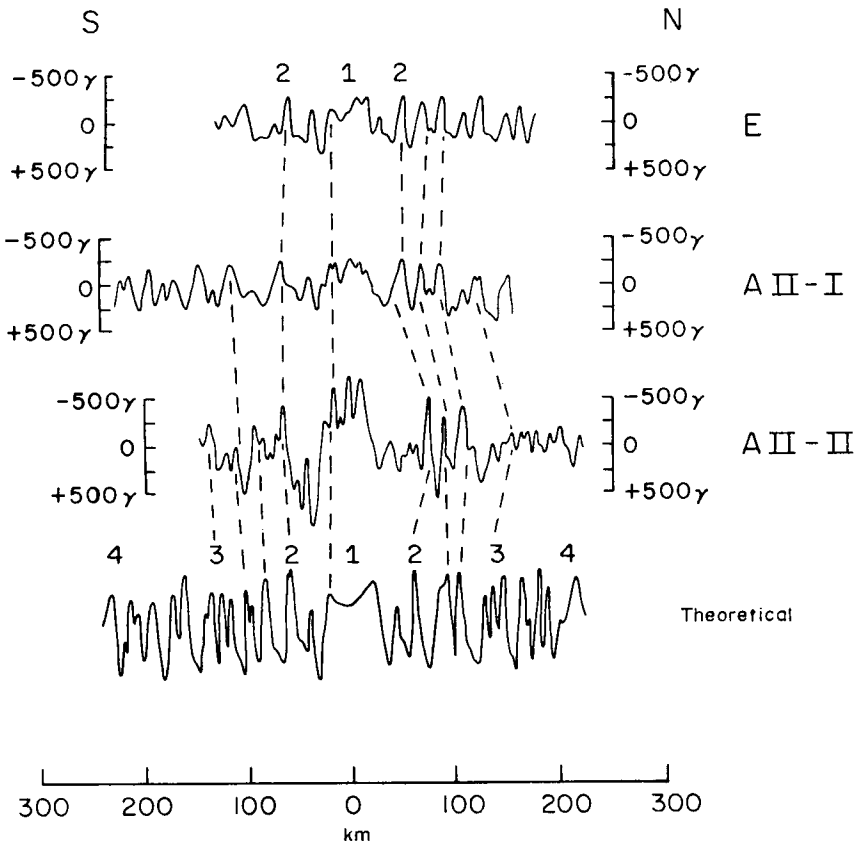

FIG. 3. Magnetic profiles: E from Grim (1970), AII-1 and AII-2 across the Galapagos Rift Zone, correlated with theoretical magnetic anomalies from Herron (1971).

formation of rocks at the ridge segment axes may be implied. We are not aware of any petrologic or magnetic studies of rock samples from either of these ridge segments.

(2) The Costa Rica Rift may have formed at a different angle at the equator which would have lowered the Costa Rica Rift magnetic intensity. However, a large rotation (~45°) would be required to attenuate the anomaly by this amount (R. Larson, private communication). Also, because the triple junction with the EPR appears not to have migrated more than 300 km westward to its present location within the past 10 My (Herron 1971), the Costa Rica Rift is probably not older than the Galapagos Rift.

Heat flow. The distribution of heat flow on the GRZ displays not only the expected decrease with distance from the crest, but also a distinct low in the region from 100 to 175 km from the crest (Fig. 4). To show the general trend of the scattered points on such a plot, we computed the mean and standard error of values in overlapping regions of 75 km width. The 75-km window gave a sufficient number of data points ($\geqslant 9$) for each interval to compensate for the bias of individually anomalous values. Table 3 displays these values in tabulated form.

Talwani, Windisch & Langseth (1971) suggest that low heat flow values on the flanks of mid-ocean ridges at ages corresponding to 6 to 10 My are characteristic of all sea-floor spreading systems and cite as evidence minima reported about the

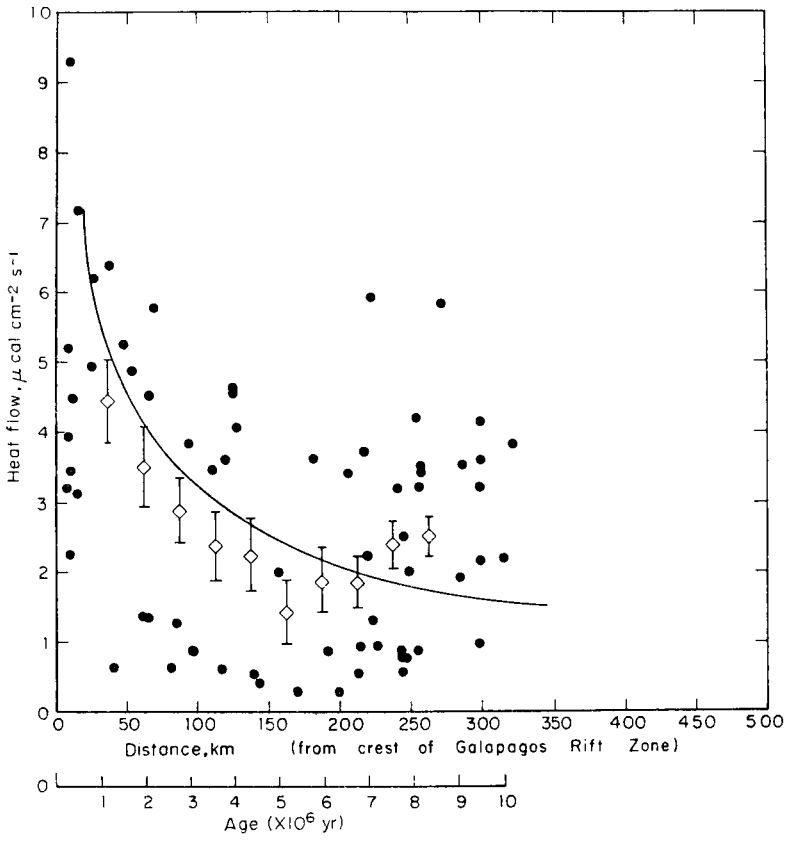

FIG 4 Heat flow versus age and distance from the crest of the Galapagos Rift Zone (spreading at 3·1 cm/yr.). Diamond symbols are arithmetic means within overlapping intervals of 75 km. Brackets represent ±1 standard error. The solid line indicates the theoretical heat flow predicted by the spreading lithospheric plate model (McKenzie & Sclater 1969).

Table 3

Heat flow—The Galapagos Rift Zone

Interval (km)	Number of points	Mean	Standard deviation	Standard error
0–75	18	4·44	2·57	·606
25–100	13	3·40	2·15	·596
50–125	13	2·88	1·73	·480
75–150	12	2·38	1·69	·487
100–175	11	2·25	1·75	·528
125–200	9	1·43	1·45	·483
150–225	12	1·87	1·70	·491
175–250	17	1·84	1·51	·366
200–275	20	2·36	1·66	·371
225–300	22	2·51	1·40	·298
250–325	16	3·11	1·18	·295

Reykjanes, Mid-Atlantic, Indian, and East Pacific Ridges. Lister (1970) also reports a low zone on the flanks of the Juan de Fuca Ridge which is of the same approximate age. McKenzie & Sclater (1969) calculate a theoretical heat flow distribution for a 75 km thick lithospheric plate cooling as it moves away from a ridge axis. Subsequent alteration of the physical parameters (Sclater & Francheteau 1970; Langseth & Von Herzen 1971) improve the fit significantly, yet this model cannot account for a heat flow variation other than a monotonic decrease with increasing age from the ridge crest. We see clearly that the GRZ low is 1·0 HFU below that predicted by the above model. Further, this low is located in crust 5 to 6 My old as Talwani *et al.* (1971) suggest, if the spreading rate is 3·1 cm/yr, as discussed above. This time scale can be used to calculate an approximate maximum depth of a possible heat sink in the lithosphere. The depth is given approximately by $\mathbf{Z} = \sqrt{\alpha t}$, where α = thermal diffusivity of the lithosphere. For $t \approx 6$ My, we find $\mathbf{Z}$ max ≈ 15 km, i.e. within the upper part of the lithosphere.

The distribution of heat flow with distance from the GRZ crest (Fig. 4) is peculiar in that most of the values are distributed in two groups: those $\geqslant$3HFU, and those $\leqslant$1·5HFU. If the low values within 250 km of the crest are omitted, we note that the cooling curve for a lithospheric plate developed by McKenzie & Sclater (1969) fits the remainder of the values reasonably well. This observation suggests that the low values have resulted from local environmental distortion. Nevertheless, we have no direct evidence for such environmental effects, and the zones of low heat flow found on other ridge flanks suggest that a common but undetermined tectonic process within the lithosphere may also contribute to some of the lows of the GRZ flanks.

East Pacific Rise. The eastern equatorial Pacific is topographically dominated by the north–south trending East Pacific Rise, which forms a continuous but very young spreading system from the Eltanin Fracture Zone at 55° S through the triple junction with the Galapagos Rift Zone at 2° N and into the Gulf of California at 25° N. Herron (1971) has utilized magnetic anomalies to define the sea-floor spreading history of this complex area. Anderson & Sclater (1971) and Sclater *et al.* (1971a) have used topographic relief to suggest that the eastern Pacific has undergone a complex reorganization in which the Mathematicians' and Galapagos Rises are fossil ridge crests which remain from an east–west 'jump' in spreading centres over the entire ridge segment from 20° N to 25° S. The smooth topographic profiles of the youthful EPR are broken abruptly by 500 m steps marking the boundary with older crust on the flanks of the fossil ridges. The complex history of oceanic crust in the entire eastern Pacific is supoprted by these independent interpretations, although the two approaches above yield different ages for the jump, 10 My BP and 5 My BP, respectively.

The EPR crestal depths vary from 2900 m at 5° to 15° S to 2700 m at 20° N. The two fossil ridges in the area have crestal depths of about 3400 metres. Menard *et al.* (1964) first reported the topographic high now called the Galapagos Rise. Our two profiles (Fig. 5) show a broad bulge of about the same general physiography as the EPR at 9° S, but none at 7° S.

Spreading rates vary from 6·0 cm/yr over the section from 25° N to 10° S, to $\geqslant$9·0 cm/yr at 20° S. There is, however, a discrepancy between spreading rates for the Galapagos Rise prior to the jump: Herron (1971) calculates 5·0 cm/yr; Anderson & Sclater (1971) calculate rates similar to those found at present on the EPR.

Heat flow. The heat flow distribution on the EPR, excluding regions of the sea floor produced by previous episodes of spreading, displays a remarkable correlation with the theoretical cooling of a lithospheric plate (Fig. 6). These results are tabulated in Table 4. Secondary highs are associated with the fossil ridges (Fig. 7).

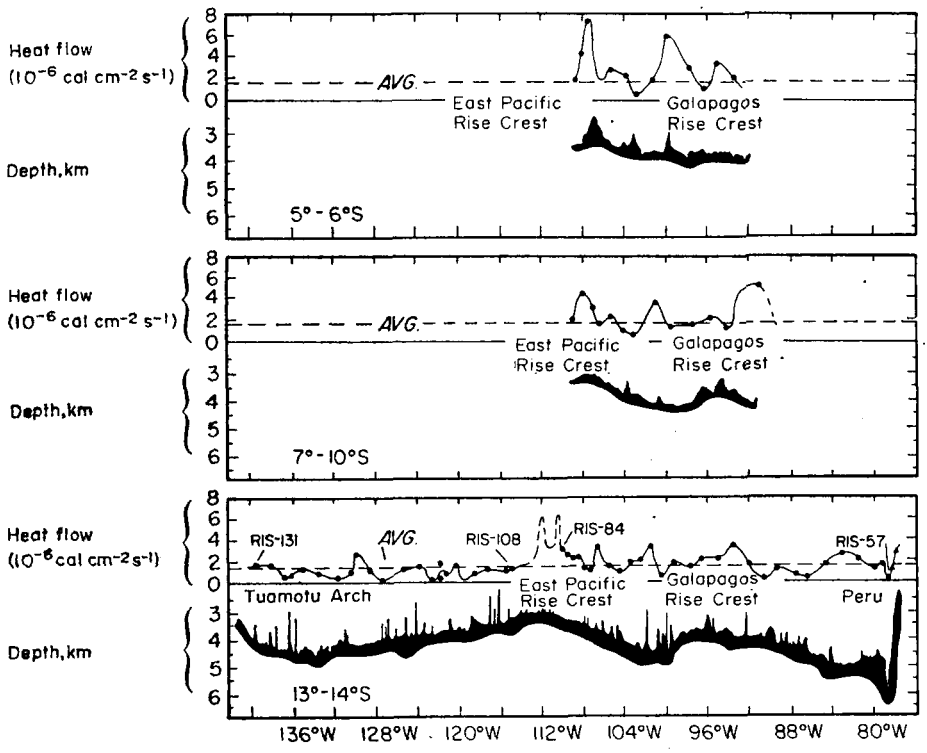

FIG. 5. Topography and heat flow profiles across the Galapagos Rise at 5°–6° S and 7°–10° S from AII-54 cruise compared to a profile at the 13°–14° S from Von Herzen & Uyeda (1963).

Table 4

Heat flow—The East Pacific Rise

Interval (My)	Number of points	Mean	Standard deviation	Standard error
0–2	46	3·04	1·97	·291
1–3	37	3·27	2·28	·375
2–4	42	3·11	2·13	·329
3–5	41	2·63	1·70	·266
4–6	22	2·16	0·94	·200
5–7	13	2·64	1·41	·391
6–8	9	1·19	1·69	·563
7–9	9	1·53	0·56	·187
8–10	12	1·70	0·56	·163
9–11	13	1·60	0·86	·237
10–12	8	1·59	0·96	·338
11–13	4	2·55	2·28	1·140
12–14	7	2·02	1·84	·695
13–15	9	1·52	0·86	·286
14–16	9	1·47	1·06	·353
15–17	7	1·56	1·19	·448

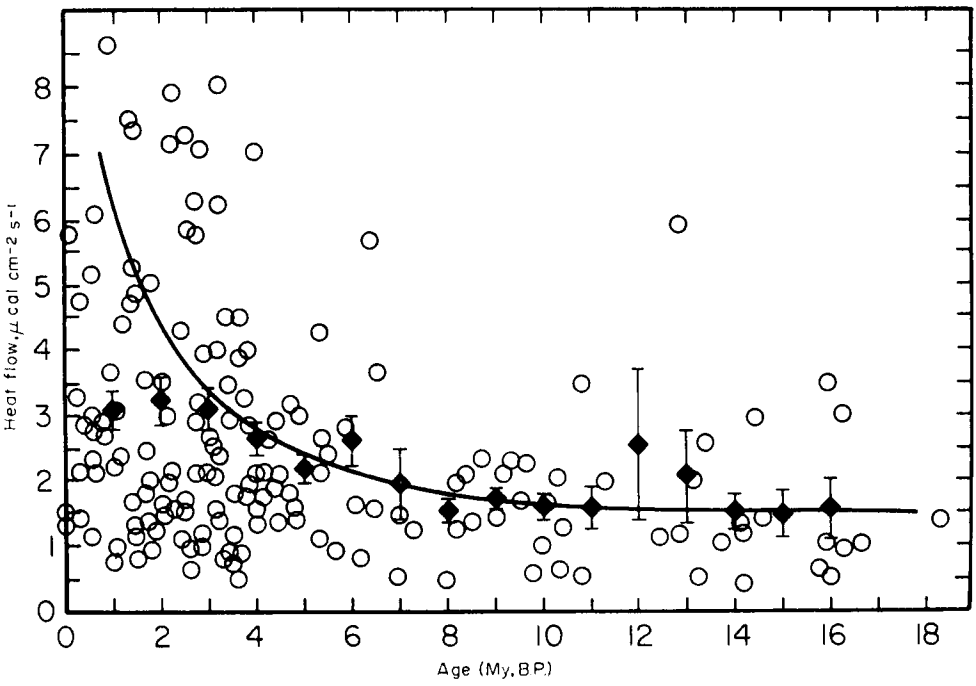

FIG. 6. Heat flow versus age for the East Pacific Rise. Arithmetic means, indicated by diamond symbols, and standard error are plotted for 2 My overlapping intervals. Data for the older sections of the ridge are taken only from those areas of the eastern Pacific where fossil ridges have not been found. The solid line indicates the theoretical heat flow predicted by the spreading lithospheric plate model (McKenzie & Sclater 1969).

In general terms, the Nasca Plate north of 15° S is an area of high heat flow. Most, but not all, of the high heat flux is associated with the secondary spreading centre in the Nasca Plate. However, there also is a zone of high heat flow south of the Carnegie Ridge in an area characterized by east–west magnetic anomalies of undetermined age (Herron 1971). We can only suggest an association of this high heat flow with that of the Panama basin, GRZ, and northern part of the Cocos Ridge. The southern Cocos Ridge and the Nasca Ridge, other aseismic features in the area, display normal to low heat flow.

The Mathematicians' Ridge is marked by two zones of equally high heat flow, one associated with the crestal province, the other 500 to 800 km to the west (Figs 1 and 7). The apparent double high may result merely from the lack of data between these maxima; the possibility exists that most of the region from 15° to 20° N and 105° to 120° W is associated with high heat flux. It seems difficult to relate such a zone to the plate tectonic model, since the heat flux predicted by this model should approximate $\sim 1{\cdot}8$ μcal cm^{-2} s (HFU), only slightly above normal.

The heat-flow maximum of the Galapagos Rise appears to be displaced from the topographic crest (Fig. 5). It is interesting to note that this zone is located over crust of the same relative age as the high on the flank of the Mathematicians' Ridge (Fig. 7). The mechanism associated with both flank highs might then be related to remanent heat sources remaining after the spreading centre jumped, possibly in the form of

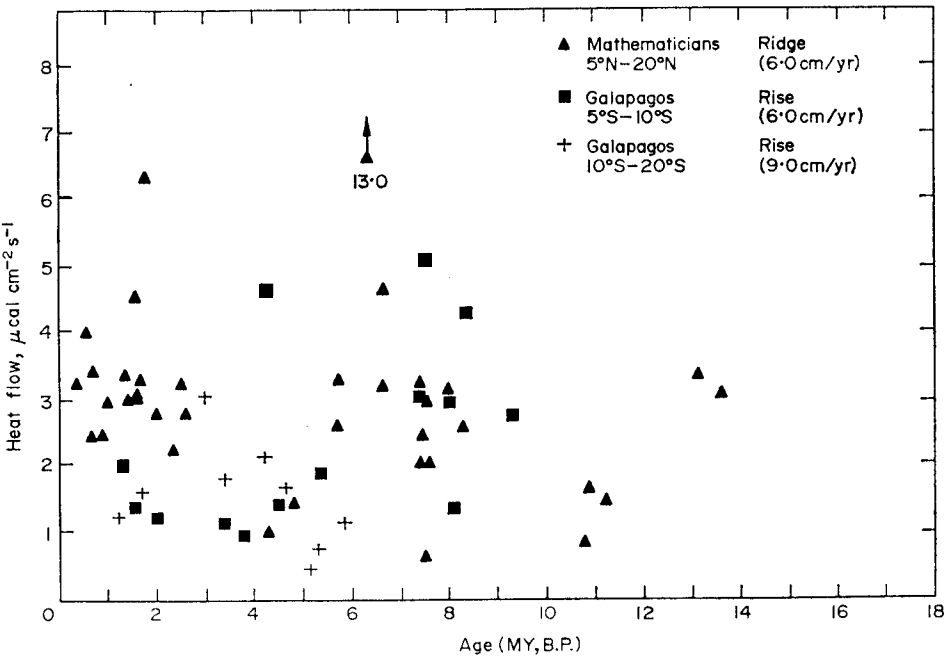

FIG. 7. Heat flow versus age (relative to zero at the crest) of fossil ridge crests in the eastern Pacific. The Galapagos Rise crestal average is ~1·5 HFU; the Mathematicians Ridge is ~2·5 HFU.

magma chambers (Herron 1971). If such exist they should be identifiable from seismic methods.

Crustal age vs. heat flow. As mentioned above, the age of spreading centre jumps in the eastern Pacific has been suggested to be either 5 or 10 My BP. If the heat-flow distribution in a lithospheric plate is governed solely by the conductive cooling in the plate (McKenzie & Sclater 1969; Sclater *et al.* 1971a), heat flow might be used as a predictor of the age of the crestal jump.

The theoretical calculations show that the heat flow at fossil ridge crests of 5 My age should be ~2·5 HFU, and that at crests of 10 My age should be ~1·6 HFU. Since the heat flow average of the crestal region of Mathematicians' Ridge is close to 2·5 HFU, and that of the crestal region of the Galapagos Rise is close to 1·5 HFU, we may infer that the former ridge jumped at 5 My BP and the latter at about 10 My BP. The time scale of such a tectonic interpretation would be a compromise between those proposed by Herron (1971) and Anderson & Sclater (1971).

Heat flow variability

A relatively large scatter in heat-flow values is almost universally characteristic of any set of measurements across or within active mid-ocean ridge crests and flanks. This characteristic first became obvious for the East Pacific from the long profiles approximately normal to the EPR crest discussed by Von Herzen & Uyeda (1963). Near the ridge crest, measurements were spaced as close as 40 km, from which a heat-flow pattern on a scale of a few hundred km could be discerned. Nevertheless, a few closer-spaced measurements showed significant scatter at a scale of a few kilometres or less for some regions, and an overall analysis of the local station environments strongly suggested a correlation with local topography and sediment

distribution. In such regions, the possibility always exists that a large-scale geographic variation will be masked or aliased by another of similar amplitude at a scale which is equal to or smaller than the spacing of measurements.

The small-scale variability on ridges has commonly been attributed to a local distortion of a uniform flux from below by irregular bottom topography and/or non-uniform distributions of sediment thickness and sedimentation rates. The sea-floor spreading model suggests that vertical mass transfer of molten rock and fluids is an important source of heat near ridge crests. The new measurements reported here (Tables 1 and 2) in part comprise data obtained by two techniques designed to investigate this problem: (1) repeated measurements made on station during ship drift, and (2) measurements place in small regions surveyed around marker buoys.

Detailed surveys. To investigate such small scale variations of heat flow, four surveys around slack-wire anchored buoys were made on AMPHITRITE and AII–54 cruises (Figs 8, 9, 10 and 11). The buoy height above the sea surface ($\approx$5 m) limited radar range and hence the extent of the surveys to within $\approx$5–7 n.m. (10–15 km) radius of the buoys, so that $\approx$300 to 400 km^2 were surveyed on each site at about 2 km line spacings. The buoy positions were established by standard celestial navigation techniques on AMPHITRITE, and by satellite fixes on AII-54; the repeatability of satellite fixes showed that the buoys of the AII-54 cruise maintained position within $\approx$1/2 n.m. (1 km) radius during the periods (2–3 days) of the survey and measurements.

The surveys made before the heat-flow measurements included broad-beam 12 kHz echo sounding and magnetics on AMPHITRITE, and also 3·5 kHz echo

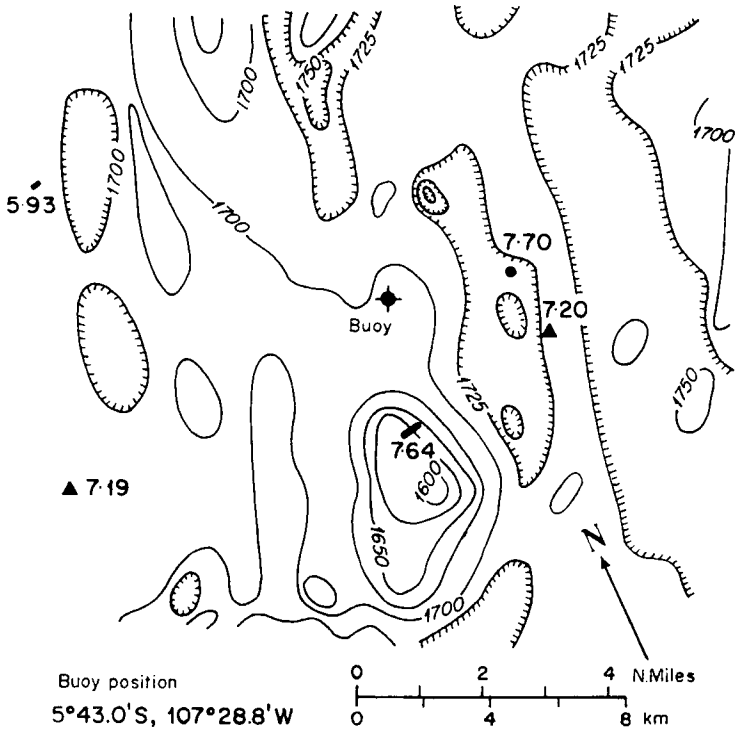

FIG. 8. Detailed topographic and heat flow survey area A, located ~70 km west of the EPR crest at 5° S. Values for heat flow are in μcal cm^{-2} s^{-1}. Solid triangles mark piston core stations, others made by the short probe. Contours are in uncorrected fathoms based upon 800 fm s^{-1} sound velocity.

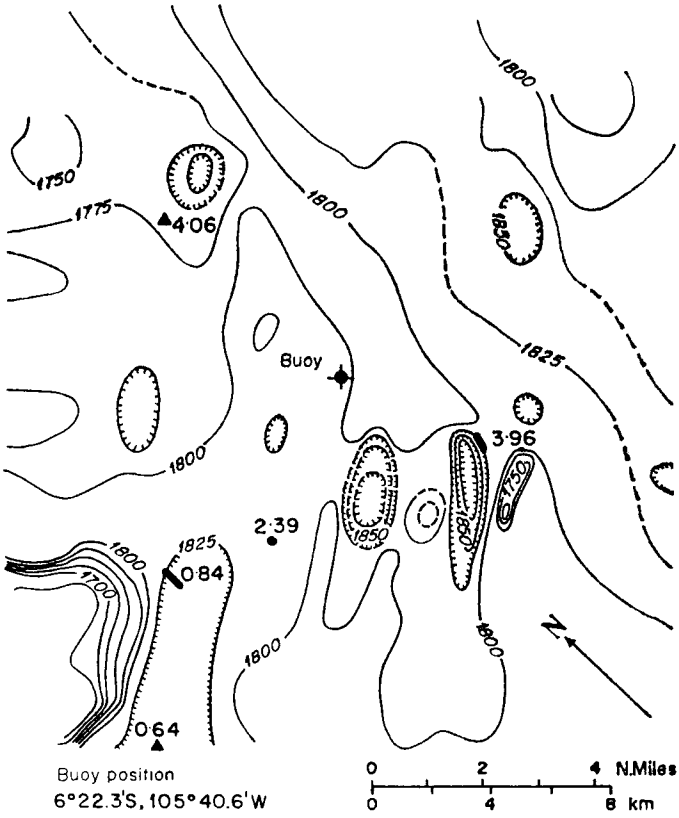

FIG. 9. Survey area B, located ~80 km east of the EPR crest at 6° S. Contours and symbols as in Fig. 8.

sounding on AII-54 cruise. Survey areas A, B, and C were all located within 100 km of the EPR crest (Fig. 1), and D on the lower west flank, of the EPR about 1400 km from the crest. The crestal surveys all indicated lineation of topography sub-parallel to the trend of the crest, best developed in Area C with a 200 fm (366 m) deep valley elongated parallel to the crest. This area also has the greatest range of heat-flow values, from 1·29 HFU in the valley to >7·29 HFU about 10 km to the east (Fig. 10). The valley floor is obviously sedimented, along with most of the region of subdued topography in the area. Rock outcrops were photographed on at least some parts of the steep valley walls. Intermediate heat flows were measured between the valley and the >7·29 HFU value to the east. At this station, the temperature gradient exceeded the scale of the recorder for all except the uppermost thermistor probe in the sediment.

Area B (Fig. 9), about 80 km east of the EPR crest, also exhibits a wide range of heat-flow (0·64 to 4·06 HFU). The lowest values are located within a small lineated depression, bordered on the north-west side by the steep flank of a 200 fm (366 m) high hill or ridge. The values increase towards the east from the depression. The highest and lowest measurements are well established with piston coring apparatus which penetrated the bottom more than 10 m with five thermistor probes at both stations. The multiple lowers with a short probe reproduced the values at each of the other stations within measurement accuracy.

Area A (Fig. 8) is within a region of relatively subdued topography (±100 fm or ±183 m) about 70 km west of the EPR crest. All the values at the five localities in area A are quite uniform and high (5·9–7·7 HFU). Such very high values have not

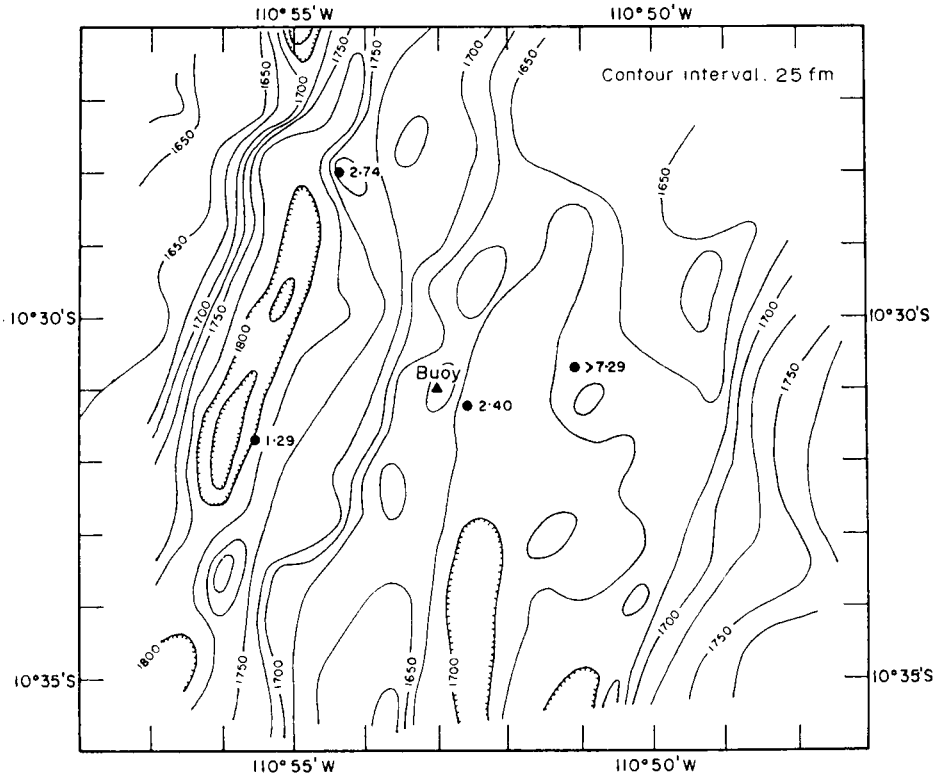

FIG. 10. Survey area C, located ~100 km west of the EPR crest at 10° S Contours as in Fig. 8. Heat flow stations indicated as filled circles.

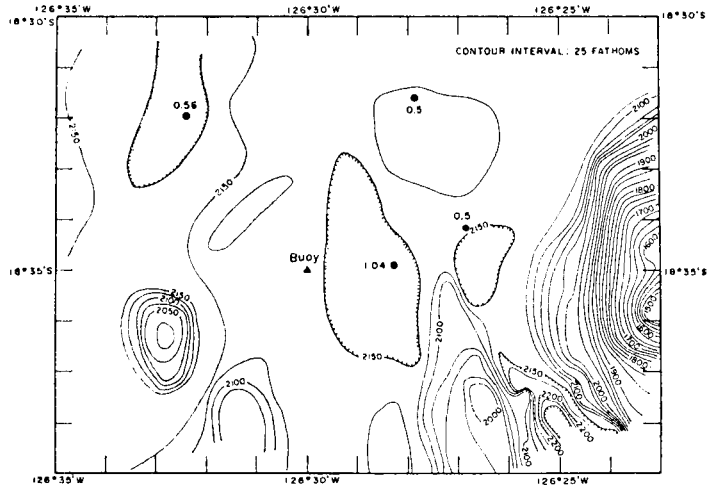

FIG. 11. Survey area D, located ~1400 km west of the EPR crest at 18° S. Contours as in Fig. 8. Heat flow stations as in Fig. 10.

heretofore been established over regions as large as area A, indicating that the highest flows on ridges are not always localized. At a spreading rate of 6 cm/yr, the heat flow for this area is close to the theoretical prediction of the spreading lithospheric plate model.

The heat-flow values of area D, on the lower western flank of the EPR, were measured in a relatively subdued sea-floor topographic setting, except for a 600 fm (1098 m) high seamount on the eastern margin of the surveyed area (Fig. 11). The subdued topography suggests sedimentary infilling from higher surrounding elevations, at least from the east. The topography is typical of the hill and valley features noted by Von Herzen & Uyeda (1963) for the EPR flank province. Except for one value within the normal range, the other heat-flow values are about half normal (0·5 HFU). It seems difficult to account for the low values by topography or distribution of sediments, unless there is a buried basement-sediment interface with significant undulations. The low values could then be explained by refraction of heat around valleys where low-conducting sediments have accumulated to greater thickness.

The measurements from areas C and B strongly suggest that topography and sediment distribution are correlated with heat-flow values. The low values measured in thickly-sedimented valleys may be explained best by rapid sedimentation (e.g. van Andel & Komar 1969) combined with refraction of heat around the low-conducting sediment bodies (Von Herzen & Uyeda 1963).

We have investigated the possible effect of sedimentation rates from the cores obtained in area B. The 7·5 and 9·0 m piston cores recovered at stations 31 and 35, respectively, have been dated by C-14 techniques. The results (Fig. 12) indicate sedimentation rates of 20 ± 3 cm/10^3 yr at station 31, and 10 ± 2 cm/10^3 yr at station 35. The C-14 ages at the tops of the sediment cores, particularly that of station 31, and the shortened lengths of recovered core compared to bottom penetration, suggest that part of the upper section of the sediments is missing in the cores, a not uncommon characteristic of the piston-coring technique (McCoy & Von Herzen 1971). The older

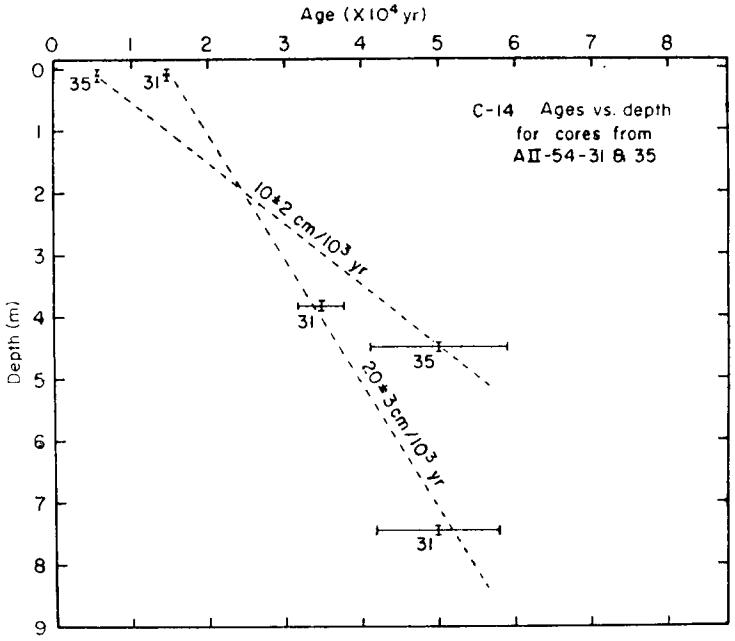

FIG. 12. Results of C-14 age dating of cores from stations 31 and 35 in survey area B. Sedimentation rates are 20 ± 3 cm/10^3 yr and 10 ± 2 cm/10^3 yr respectively.

ages at the tops of the cores may also be consistent with the hypothesis that a slumped block of sediments were cored, as discussed below.

At a steady half-rate of sea-floor spreading of 6 cm/yr, the basement rocks in area B, 80 km from the EPR crest, should have an age of about $1{\cdot}3 \times 10^6$ yr. At steady sedimentation rates of 10 and 20 cm/10^3 yr, the uncompacted sediment thicknesses at stations 31 and 35 should be 130 and 260 m, respectively. These are not unreasonable thicknesses, although we have no data to verify them. The higher sedimentation rate at station 31 may result from local ponding of sediments derived from a region about twice as large as the pond (e.g. van Andel & Komar 1970), probably including the steep slope to the west. Von Herzen & Uyeda (1963) have shown that even such relatively high sedimentation rates cannot produce more than a 10 per cent reduction in the equilibrium heat flux, and can in no way account for the difference (a factor of 6) in measured heat flow between the two stations.

A tilted sedimentary slump block, which could have slid from the nearby hill to the north-west, might be invoked to explain the relatively low gradient at station 31 (Fig. 13). The block would have had to remain relatively coherent during the sliding process to produce the apparently uniform increase of sediment age with depth by the C-14 method. Even if the block were 100 m thick, however, a heat-flow reduction by a factor of 6 would require the measurement to have been made $\leqslant 10^3$ yr after occurrence of the slump (Von Herzen & Uyeda 1963, Fig. 11). This seems unlikely in view of the crustal age of region B, which is at least a factor of 10^3 greater than this.

Von Herzen & Uyeda (1963, p. 4239) have suggested that nearby values on the EPR which differ by a similar ratio may be explained by a combination of heat-flow refraction and more rapid sedimentation. Low values measured in a similar topographic situation to that of station 31 in the north-east Pacific (Sclater, Mudie & Harrison 1970) have also been explained as a combination of refraction and sediment slumping. Sclater *et al.* (1971b) have shown that sharp topographic irregularities can be associated with marked local depression of the regional heat flux, although the effect of any sediment cover is to attenuate such anomalies. Station 31 does not appear to be located near enough to a major topographic feature to explain the heat-flow anomaly by topography alone; however, we cannot exclude topography undetected by the survey grid or by the limitations inherent in echo-sounding from a surface ship.

Although we have no definite evidence that local environmental effects have significantly lowered the equilibrium heat flow at station 31, the low value is inconsistent with the plate tectonic model. Hence, the regional heat flux in area B is probably close to 4·0 HFU, the values measured at stations 32 and 35. That for area C is difficult to determine other than the average of values outside of the prominent valley (4·1 HFU). In such topographic situations, particularly on ridge crests, it appears imperative to obtain closely-spaced measurements in topographically surveyed regions in order to obtain representative values.

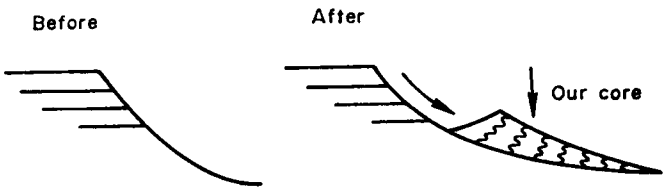

FIG. 13. Schematic diagram of mechanism of possible semi-coherent sediment slumping at station 31.

Repeated measurements. On AMPHITRITE and AII-54 cruises, there were 23 stations at which more than one measurement was obtained during the time on station while the ship was drifting. At some stations with many measurements (e.g. station 20, AII-54) the drift over the bottom may have extended over several kilometres, but for most stations with only 2 or 4 measurements, the drift was likely limited to a few hundred metres or less. Therefore, these measurements can provide data on the variability of heat flow over short distances.

Von Herzen (1964) computed an overall standard deviation for groups of values, defined as

$$\sigma^2 = \frac{\sum_{i=1}^{K} n_i s_i^2}{\sum_{i=1}^{K} n_i - K} \tag{1}$$

where n_i = number of measurements at station i with standard deviation s_i, and the number of stations is K. In our study, the heat flow varies substantially between stations, and some evidence has accumulated that the standard deviation is proportional to the magnitude of the heat flow (e.g. Langseth & Von Herzen 1971, Fig. 13). To include stations with different heat flux together in a more comparable way, we have modified equation (1) as

$$\sigma^2 = \frac{\sum_{i=1}^{K} n_i \left[\frac{s_i}{m_i}\right]^2}{\sum_{i=1}^{K} n_i - K} \tag{2}$$

where m_i is the mean value at station i. σ in equation (2) is then a fractional standard deviation.

The value of σ computed for the AMPHITRITE and AII-54 stations with more than one measurement is 0·36. This figure is at least twice as large as that found at repeated stations by Von Herzen (1964), and much of the increase can be attributed to a few stations with a relatively large number of variable measurements (e.g. station 20, AII-54). Arbitrary exclusion of only three of the 23 stations (stations 13 and 20, AII-54; stations 38–39, AMPHITRITE) gives $\sigma = 0{\cdot}18$, which for an average heat flow of 2·0 HFU, is about the same as that found previously. Obviously the station variability changes enormously between different stations. At some (stations 11, 22, 26, 27, 28, 32, AII-54 cruise), the measurement variability is within instrumental error. Some, but not all, stations with three or more measurements show that the heat flow appears to vary systematically with successive measurements (station 20 is again a good example). These imply that local environmental disturbances and/or heat sources on a scale of a few tenths to a few kilometres are significant, as might also be deduced from the measurements obtained in detailed survey areas discussed above. If the values in each of the four detailed survey areas are considered in the analysis as variability at four stations, σ is somewhat increased to 0·38. Further increases would be expected as the area of the ' station ', or sample region, is increased in size.

Bottom water temperature profiles Vertical temperature profiles of near bottom water in the East Pacific are not uniform, but vary with geographic position, depth, and perhaps other environmental parameters. Certain features are characteristic of

many of the profiles, however, and these are typified by the deep water profile illustrated in Fig. 14 (AMPH-10). The temperature reaches a minimum several hundred metres above the sea floor, increasing below that along a gradient which is close to adiabatic (≈0·13° C/km). Within a few metres to a few tens of metres above the bottom, the gradient frequently appears to be superadiabatic; this unexpected phenomenon is discussed below.

Before attempting to analyse the similarities or differences between stations, it is necessary to assess the accuracy and precision of the water temperature profiles. On AMPHITRITE cruise, the lack of absolute temperature calibrations of thermistors only permitted relative water temperatures to be measured. Thus, on all AMPHITRITE profiles, water temperatures are plotted relative to those measured when the apparatus had penetrated the bottom. The stability and accuracy of the records allowed temperatures to be measured with a relative accuracy of a few millidegrees C on both AMPHITRITE and AII-54 cruises. Height above bottom was measured in all cases by the difference in acoustic (12 kHz) travel time between the direct and bottom-reflected signals from a pinger attached near the apparatus. Acoustic velocities have been corrected by Matthews' (1939) tables, and geometric corrections are usually negligible. For AMPHITRITE cruise, the largest source of error is the lack of a precision time base for the temperature records, permitting a few per cent systematic uncertainty in height above bottom because of the uncertainty in correlation of time with the pinger records. On AII-54 cruise, this uncertainty did not exist because the acoustic telemetering of data was recorded together with height above bottom.

Two critical tests of the accuracy of the measurements are to compare (1) the 'up' and 'down' portions of profiles at a single station, and (2) the relative profiles between nearby stations. The 'down' portions of the recordings usually extend only a few metres above bottom on AMPHITRITE cruise because of a time delay in instrument turn-on, and are frequently degraded on AII-54 cruise because of rapid lowering speeds and/or poor bottom acoustic reflections. Hence, we have emphasized

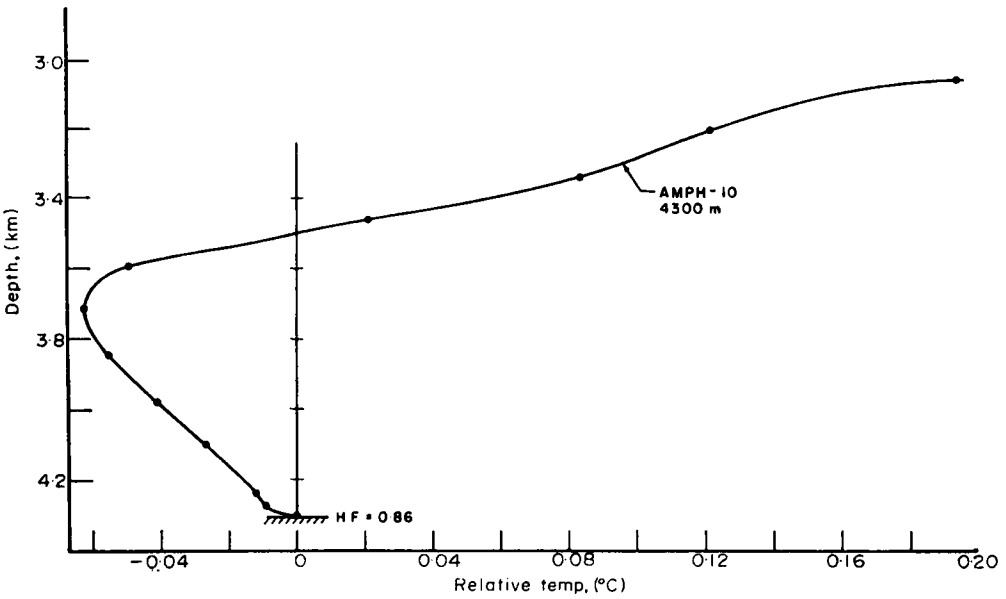

FIG. 14. Deep water temperature profile at station 10, AMPHITRITE cruise, west of the East Pacific Rise crest (Pacific plate). Temperature relative to that measured at bottom. Water depth 4300 m, heat flow = 0·86 HFU.

comparisons between nearby stations, usually the 'up' portions of the records. Profiles from nine such localities on both are illustrated in Fig. 15. With few exceptions, the general shape of the temperature-depth profiles is similar for any locality. Relative temperatures are within $\pm 0{\cdot}01$ °C except near the bottom at some stations. Notable exceptions are: (1) Profile AMPH-43, which deviates significantly from the profiles obtained from three other stations at this locality; (2) profiles at AMPH-50; and (3) profiles at AMPH-51. The profile inconsistencies at these localities seem most likely the result of timing inaccuracies in the temperature records, as discussed above, because the slopes of linear portions of the comparative profiles, are different although the overall profile shapes are similar. The only other major difference is for station 47, where the two profiles appear to have significantly different slopes for 500–600 m above bottom, but similar slopes above 3·6 km depth; this discrepancy is not obviously explained. These comparisons between nearby measurements indicate sufficient instrumental consistency for the qualitative and semi-quantitative discussion which follows.

Depth of minimum temperature. Although it is not feasible to illustrate water temperature profiles for each station of AMPHITRITE and AII-54 cruises, most of the profiles show a minimum temperature a few hundred metres above bottom (Fig. 15), below which the temperature increases approximately along an adiabatic curve to the bottom except for a frequently measured increased gradient a few metres above the bottom interface (discussed below). Table 5 gives the minimum *in situ* temperature (for AII-54 cruise) and depth of the minimum temperature for each station. An adiabatic increase of temperature near the bottom indicates a homogeneous, neutrally stable water layer. The homogeneity may be attributed to mixing, as a result of turbulence, bottom heat flux, or other undetected mechanisms. Topographic isolation of bottom water has been associated with such water temperature profiles at some Pacific localities (Craig *et al.* 1970).

The data show that the depth to the temperature minimum decreases from nearly 5 km in the central Pacific (station AMPH-55), consistent with the data of Chung *et al.* (1969), to a depth less than 3 km near the EPR crest. The EPR and Nasca Ridge must act as a barrier to renewal of bottom water at depths greater than about 3 km over the Nasca plate, because the depth to the temperature minimum is not much greater than this for every station in this region. The influence of the EPR barrier is clearly shown in a plot of water layer thickness beneath the temperature minimum *vs.* water depth (Fig. 16). Except for stations at which temperature decreases all the way to the bottom (layer thickness zero) and two other anomalous stations, the values over the Pacific plate are clearly separated from those over the Nasca plate by an appropriate line with a slope of 1 on such a plot. One of the anomalous stations (AII-54-15) may be located in or near a fracture zone (Menard 1966; Herron 1971; Anderson & Sclater 1971) which may extend the influence of the Pacific plate bottom water east of the EPR crest. The line with slope 1 which divides the Pacific plate and Nasca plate measurements intersects the water depth axis at about 3350 m; this may be close to the effective sill depth of the EPR. Similarly, the one reliable measurement in the Panama Basin (AII-54-55) suggests that the sill depth is even shallower there.

If the deep water temperature structure were horizontally stratified at any locality, then straight lines between the connected points of stations at the same locality in Fig. 16 would also have a slope of 1. In detail there is no such uniformity of slope, although there is a tendency of all such stations (except where W = O) to have such a mean slope. It is not clear to what extent the variations represent local water structure or uncertainties in the temperature measurements.

The influence of water movement and bottom topography on bottom water mixing is illustrated by a series of near-bottom profiles across the EPR at 18° S (Fig. 17). Here the thickness of the bottom mixed layer remains relatively constant

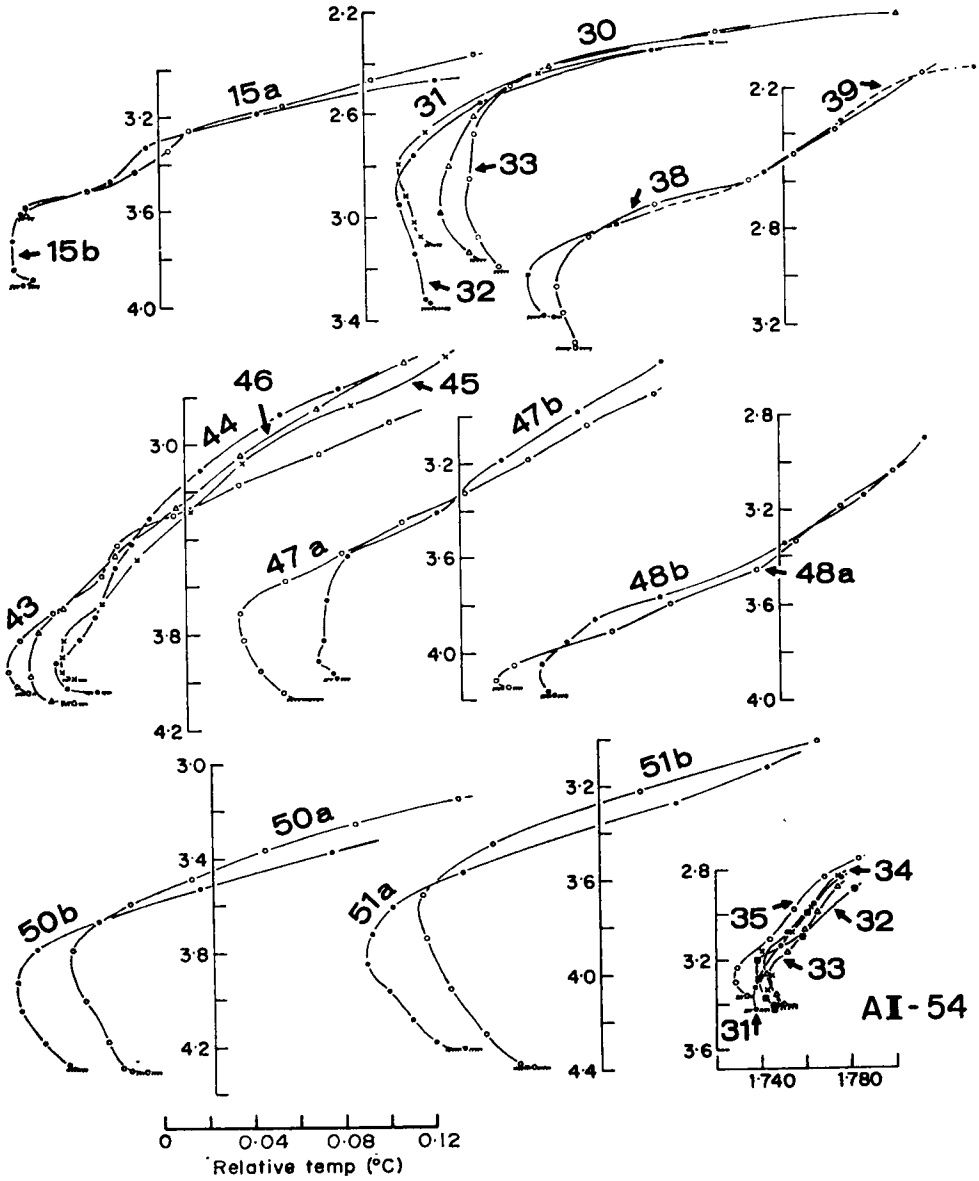

FIG. 15. Near bottom water temperature profile comparison for nine localities in the central East Pacific. Curves are drawn between measured points as shown. Depths given in metres (corrected) below sea level. Relative *in situ* temperature scale applied to all profiles; absolute temperatures measured for lower group on right side (AII-54 cruise, area 'B', Figs 1 and 9). Profiles adjusted horizontally at each locality on AMPHITRITE cruise for best fit of curves above a few metres above the sea floor. 'a' and 'b' following AMPHITRITE station numbers indicate separate instrument lowerings at the same location.

on the west flank, increasing in elevation with the topography. East of the crest, the depth to the top of the mixed layer remains relatively constant irrespective of bottom depth (Table 5). These observations seem best explained by moderate mixing through interaction with the bottom of a layer a few hundred metres thick, and eastward flow of bottom water from the Pacific plate across the EPR sill into the Nasca plate basin (namely, Knauss 1962).

On the other hand, the profiles across the EPR near 8° S show that the temperature minimum intersects the bottom as deep as 3·5 km (Table 5) west of the crest. These indicate a stability of the water column which is not affected by the bottom depth, suggesting that bottom heat flux, rather than interaction of bottom currents and topography, might be controlling the mixing of the bottom layer. Where the rate of

Table 5

Minimum in situ *water temperature* (*T min*) *and depth of T min measured on vertical profiles above bottom*

AMPHITRITE*

Sta. No.	Depth of T min (m)	Sta. No.	Depth of T min (m)	Sta. No.	Depth of T min (m)
2	4090	22	3140	41	3390
3	4310	23	2800	42	3510
5	3970	24	2650	43	3930
6	3860	25B	2910	44	3920
8	3785	26	2840	45	3870
9	3870	27	2985	46	3920
10	3700	28	3070	47A	3850
11	3680	29	3120	47B	4000
12B	3960	30	2940	48A	3900
13	3810	31	2760	48B	3890
14	3825	32	2835	49	3820
15A	(3615)	33	2700	50A	3800
15B	3760	34	2770	50B	3890
16	3450	35	2590	51A	3910
17	(3470)	36	2835	51B	3720
18	(3395)	37	3020	54B	4720
19	(3315)	38	3050	55	4950
20	(3300)	39	2980	56	4545
21	3180	40	3190	61	3650

*No absolute temperatures measured on AMPHITRITE.

AII-54

Sta. No.	T min (°C)	Depth of T min (m)	Sta. No.	T min (°C)	Depth of T min (m)
3	1·762	3000	29	1·660	(3190)
5	1·775	3160	30	1·773	2800
9	1·774	3145	31	1·740	3375
14	1·751	3195	32	1·739	3225
15	1·736	3425	33	1·740	3260
17	1·761	3200	34	1·748	3195
18	1·763	3100	35	1·733	3280
19	1·762	2975	38	1·747	3245
20	1·748	(3170)	41	1·735	3060
26	1·690	(3145)	46	1·750	3000
27	1·690	(3220)	49	1·769	3100
28	1·680	(3195)	50	1·754	3025
			55	2·027	2625

Note: Values in parentheses indicate minimum temperature coincides with bottom depth.

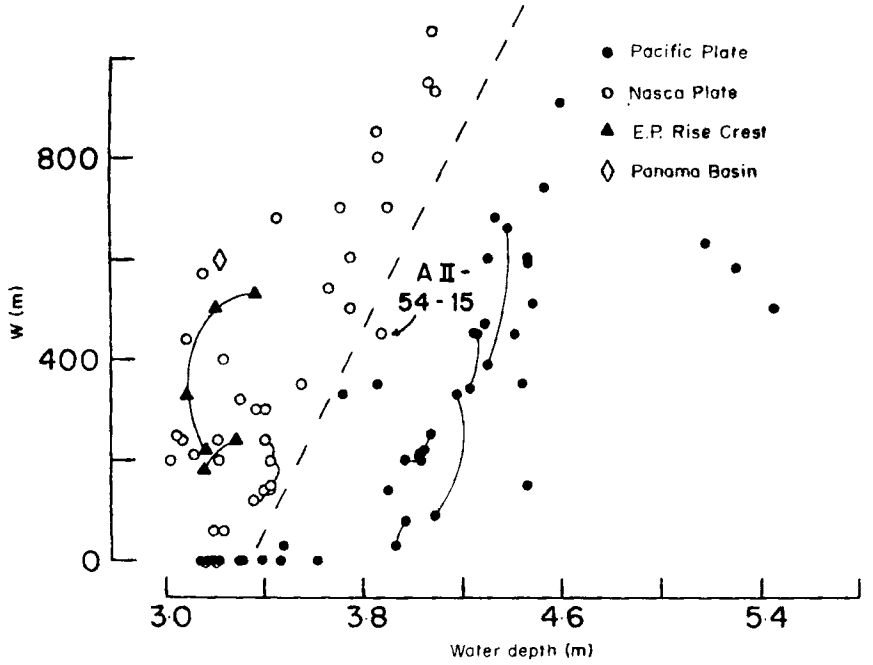

FIG. 16. Water layer thickness, W, below the depth of the temperature minimum, vs. water depth (Table 5). Symbols connected by curves represent separate profile measurements at the same locality or station.

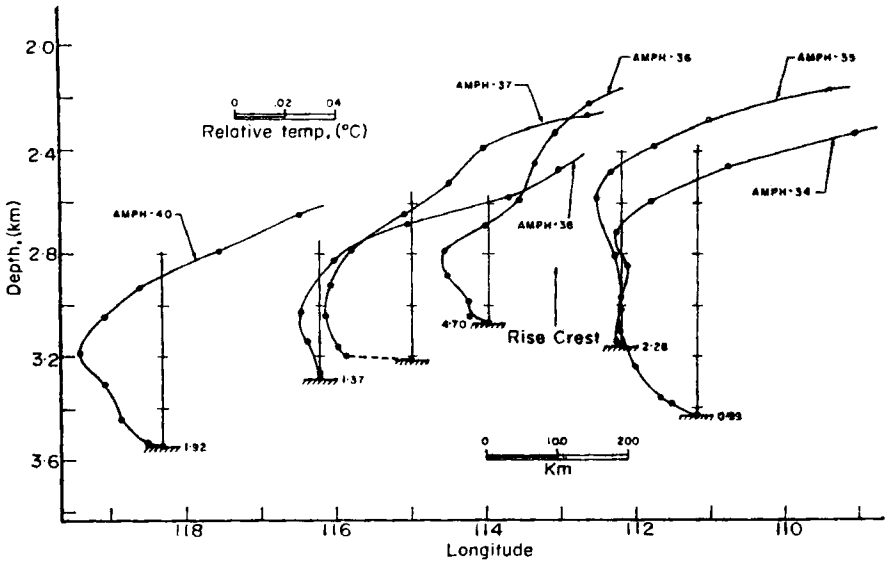

FIG. 17. Relative water temperature profiles across the East Pacific Rise crest at 18° S latitude. Heat flow (HFU) given at base (hachured) of each profile.

bottom water renewal is more rapid, as may be inferred at 8° S, the mixing caused by heat flow through the bottom may be masked (absorbed) by the advected water.

Other less obvious and perhaps local effects of heat flow on bottom water temperature structure are suggested by detailed measurements over surveyed regions. Stations 31 to 35 of AII-54 cruise were all located within a 400 km^2 area ('B' in Fig. 1). Except for station 31, all profiles show a similar shape (Fig. 15), with a characteristic minimum temperature observed at about the same depth (3250 ± 50 m). Station 31 appears to have none, or only a slight minimum which may be present at a greater depth. We note that an unusually low heat flow was measured at this station (0·64 HFU), and perhaps this locally low flux may be related to the water temperature profile anomaly in comparison to the nearby stations.

Near bottom currents have been inferred by Edmond, Chung & Sclater (1971) in the NE Pacific. Other than the generally eastward flow of bottom water across the EPR, our profiles do not suggest any marked differences over the eastern equatorial Pacific. Probably the bottom water circulation is rather sluggish compared to other parts of the Pacific.

Superadiabatic gradients. One of the basic assumptions in oceanic heat-flow measurements is the constancy with time of temperature at the sea bottom interface between water and sediments. Whereas this assumption has been generally verified to sufficient accuracy by heat-flow measurements in the oceans at depths greater than 2–3 km, some measurements and theoretical calculations indicate that the near-bottom waters are not the equivalent of an infinite heat sink of constant potential temperature for the conduction of heat through the bottom. Some measurements in near-bottom waters (Lubimova, Von Herzen & Udintsev 1965; Bodvarsson, Berg & Mesecar 1967) have indicated superadiabatic gradients in the lowermost few to few tens of metres, implying finite vertical eddy diffusivities of the order of 10^{-1} to 10^{-2} cm^2 s^{-1}. Similarly, detailed studies of the distribution of radon have resulted in values of vertical diffusivities as low as about 1·5 cm^2 s^{-1} in the lowermost few tens of metres (Broecker & Cromwell 1967).

Theoretical analysis (Wimbush & Munk 1971) suggests that, depending on current velocities, velocity shear of near-bottom water, and bottom heat flux, successive layers above the sea floor may exist through which heat is transferred from below by different physical processes. Above a layer a few centimetres thick which is stable for heat transfer by molecular conduction, a mixed mode of convective transfer may persist to heights of several metres above the bottom with gradients in excess of adiabatic by factors of 0·1 to 1. Such superadiabatic gradients have been recently observed with some very precise apparatus (Wimbush 1970). For sea water of uniform composition and potential density, there are no theoretical reasons to expect noticeable superadiabatic gradients above this mixed-mode layer (>few metres height).

In view of some previously published data from Expedition AMPHITRITE, which were used as examples of hyperadiabatic temperature gradients close to the sea floor (Lubimova, Von Herzen & Udintsev 1965), we have examined all AMPHITRITE and AII-54 cruise stations on which good data were obtained of temperature vs. height above the sea floor (or depth). Unfortunately, the basic data from the particular stations used by Lubimova *et al.* as examples of hyperadiabatic gradients were not well established (their Figs 2, 3, and 4), and none of those AMPHITRITE stations have been used in the present analysis.

Our analyses of AMPHITRITE stations on which reliable data were obtained indicate 'apparent' superadiabatic gradients, as summarized in Table 6. The extent of penetration was deduced from the sediment temperature gradient combined with the thermistor probe spacing relative to the base plate of the apparatus, or from the mud smear on the core barrels. Both techniques give a typical measurement accuracy of penetration to a few decimetres (McCoy & Von Herzen 1971).

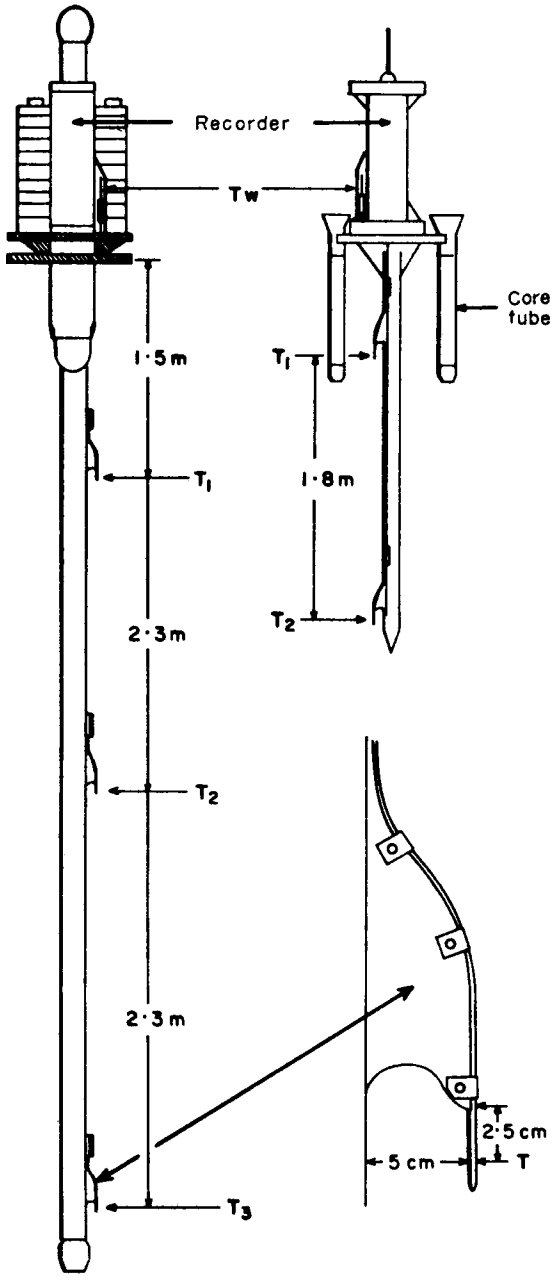

FIG. 18. Heat-flow apparatus utilized on AMPHITRITE Expedition. Piston-coring apparatus to left, and short probe and details of thermistor probe at right. T_w indicates thermistor probe used for water temperature measurements.

Table 6

Summary of bottom water temperature gradients for AMPHITRITE stations

Bottom penetration: F (or >F)		P	Indeterminant	Total
>Adiabatic gradient	15	23	1	39
⩽Adiabatic gradient	5	12	1	18
Total	20	35	2	57

Bottom penetration of apparatus: F = full, P = partial

We have separated the measurements as shown in Table 6 because the small distance (few decimetres) of the water thermistor above the base plate for the AMPHITRITE apparatus could produce 'apparent' superadiabatic gradients if the water thermistor penetrated the bottom on full penetration. Nevertheless, the table shows that a greater number (although not a greater fraction) of superadiabatic gradients were observed with partial, rather than full, penetration, where the water thermistor clearly did *not* penetrate the bottom sediments.

The average thickness of the superadiabatic layer above the bottom for the 39 stations of AMPHITRITE at which it was observed is 27 m, with a range from 8 to 140 m. The observed thickness represents an upper limit at most stations because of the ≈1-min interval between water temperature measurements during hoisting of the apparatus. The thickness of the superadiabatic layer at many stations was determined by only the first temperature measurement after pullout from the bottom. Only at stations 2, 34 and 49 were layer thicknesses greater than 50 m.

In contrast to the majority of stations of AMPHITRITE at which superadiabatic gradients were observed, only two stations (9 and 55) of 25 on which bottom water temperature data were obtained on AII-54 cruise gave superadiabatic gradients. At these two stations, the layers were ⩾50 m thick. How, then, can we explain the large discrepancy between the numbers of stations at which superadiabatic gradients were apparently measured on AMPHITRITE compared with those of AII-54 cruise? Several possibilities are suggested: (1) consistent instrumental errors were present in the AMPHITRITE data. This possibility seems unlikely in view of the different instruments used on this cruise, and the similarity of heat-flow values with others previously measured in the same regions. (2) AMPHITRITE measurements were located mostly above the Pacific plate *west* of the EPR crest, whereas AII-54 cruise measurements were mostly in the Nasca plate–Panama Basin *east* of the EPR crest. We have presented evidence that the EPR is a barrier to water flow at depths ⩾3 km. However, there is no obvious *a priori* reason why superadiabatic gradients should exist near the bottom to the *west*, rather than the *east*, of the EPR crest, despite the small systematic differences in absolute temperatures between these regions. Full bottom penetration was achieved on four of the six stations of AMPHITRITE cruise *east* of the EPR crest which exhibited superadiabatic layers. This observation suggests another explanation. (3) The water thermistor on the apparatus of AMPHITRITE cruise was located about 0·5 m lower, with respect to the base plate, than that on the corresponding AII-54 cruise apparatus. Even for those stations at which full penetration was not achieved, the lower position of the water thermistor may have penetrated a bottom boundary layer with a superadiabatic temperature gradient more frequently on AMPHITRITE cruise, with a thickness of decimetres to metres in accord with theoretical expectations (Munk & Wimbush 1971).

Synopsis

The major results and conclusions of this study of the eastern equatorial Pacific are:

(1) Where major changes in the tectonic pattern have not occurred during the past 5–10 My the correlation of heat flow vs. age of the sea floor for the East Pacific Rise matches well with theoretical plate tectonic models for inferred sea-floor ages between 3 and 18 My.

(2) The heat flow distribution and magnitude suggests relic spreading centres for the Mathematicians' Ridge and Galapagos Rise at which spreading was terminated 5 and 10 My ago, respectively.

(3) The heat flow on the E–W trending Galapagos Rift Zone is bimodal, with most values either $\leqslant 1{\cdot}5$ HFU or $>3{\cdot}0$ HFU. If the low values within 250 km of the crest are ignored, the remainder fit closely to theoretical plate tectonic models with suitable smoothing.

(4) Three surveyed areas around anchored buoys on the crestal and flank regions of the East Pacific Rise indicate substantial heat-flow variability associated with topographic irregularities. Relatively uniform (± 15 per cent) and high heat flow (6–7 HFU) was measured in a fourth area (A) near the Rise crest with relatively smooth topography. Closely-spaced measurements (within a few kilometres) frequently give smoothly-varying values between successive measurements; the observed differences at stations range up to a factor of 8, with an overall fractional standard deviation of 20 per cent.

(5) Near-bottom water temperature profiles clearly show the sill depth over the Nasca plate at about 3·2 km. The East Pacific Rise crest bars the eastward flow of Pacific bottom water. Superadiabatic temperature gradients have been observed within a few metres of the sea floor at many stations.

Acknowledgments

We are indebted to the ships' officers, crews, and scientific parties of Expedition AMPHITRITE (Scripps Institution of Oceanography) and AII-54 cruise (Woods Hole Oceanographic Institution) for the support required to make the heat-flow measurements. These cruises were supported by U.S. Office of Naval Research contracts Nonr 2216 (23) and CO-241 with the respective institutions, and by grants G-22629 and GA-1077 with the U.S. National Science Foundation. We thank Dr G. Bien for the C-14 dating provided on core material, and Dr J. Sclater for unpublished heat-flow data in the East Pacific.

Woods Hole Oceanographic Institution,
Woods Hole,
Massachusetts 02543

Roger N. Anderson is now at:
Scripps Institution of Oceanography,
La Jolla,
California 92037

References

Anderson, R. N., 1971. *A geophysical study of the Eastern Equatorial Pacific,* unpublished M.Sc. Thesis, University of Oklahoma.

Anderson, R. N. & Sclater, J. G., 1971. Topography and the evolution of the Southeastern Pacific—0°–20°S, *Earth Planet. Sci. Lett.*, in press.

Bodvarsson, G., Berg, J. & Mesecar, R., 1967. Vertical temperature gradient and eddy diffusivity above the ocean floor in an area west of the coast of Oregon, *J. geophys. Res.*, **72**, 2693–2694.

Broecker, W. S., Li, Y. S. & Cromwell, J., 1967. Radium-226 and Radon-222: Concentration in Atlantic and Pacific Oceans, *Science*, **158**, 1307–1310.

Bullard, E. C., Maxwell, A. E. & Revelle, R., 1956. Heat flow through the deep sea floor, *Adv. Geophysics*, **3**, 153–181.

Chung, Y., Bell, M. L., Sclater, J. G. & Corry, C., 1969. *Temperature data from the Pacific abyssal water*, Ref. 69–17, Scripps Institution of Oceanography, Univ. California, 75 pp.

Craig, H., Sclater, J. G., Chung, Y., Edmond, J. M., Kroopnick, P. M.& Weiss, R. F., 1970. Geochemical and temperature profiles in Equatorial Pacific bottom water (abstract), *Trans. Am. geophys. Un.*, **51**, 326.

Deffeys, K. S., Hey, R., Johnson, L. & Lowrie, A., 1971. Plate tectonics near the Galapagos triple junction (abstract), *Trans. Am. geophys. Un.*, **52**, 237.

Grim, P. J., 1970. Connection of the Panama fracture zone with the Galapagos rift zone, eastern tropical Pacific, *Mar. geophys. Res.*, **1**, 85–90.

Edmond, J., Chung, Y. & Sclater, J. G., 1971. Pacific bottom water flow: implications of continuous deep water temperature profiles from the central North Pacific, *J. geophys. Res.*, in press.

Herron, E. M. & Heirtzler, J. R., 1967. Sea-floor spreading near the Galapagos, *Science*, **158**, 775–779.

Herron, E., 1971. Sea-floor spreading and the Cenozoic history of the east central Pacific, *Geol. Soc. Am. Bull.*, in press.

Horai, K., 1969. Cross-coveriance analysis of heat flow and seismic delay times for the earth, *Earth Planet. Sci. Lett.*, **7**, 213–220.

Horai, K. & Simmons, G., 1969. Spherical harmonic analysis of terrestrial heat flow, *Earth Plant. Sci. Lett.*, **6**, 386–394.

Kaula, W. M., 1966. Tests and combinations of satellite determinations of the gravity field with gravimetry, *J. geophys. Res.*, **71**, 5303–5314.

Knauss, J. A., 1962. On some aspects of the deep circulation of the Pacific, *J. geophys. Res.*, **67**, 3943–3954.

Langseth, M. G., 1965. Techniques of measuring heat flow through the ocean floor, in *Terrestrial Heat Flow, Geophysical Monograph* #8, ed. by W. H. K. Lee, *Am. geophys. Un.*, 58–77.

Langseth, M. G. & Von Herzen, R. P., 1971. Heat flow through the floor of the world oceans, in *The Sea, vol. 4, part* 1, ed. by A. E. Maxwell, Wiley-Interscience, 299–352.

Lister, C. R. B., 1970. Heat flow west of the Juan de Fuca Ridge, *J. geophys. Res.*, **75**, 14, 2648–2654.

Lubimova, E. A., Von Herzen, R. P. & Udintsev, G. B., 1965. On heat transfer through the ocean floor, in *Terrestrial Heat Flow, Geophysical Monograph* #8, ed. by W. H. K. Lee, *Am. geophys. Un.*, 78–86.

Matthews, D. J., 1939. *Tables of the velocity of sound in pure water and sea water*, Hydrographic Department, Admiralty (London), H.D., 282, 32 pp.

McCoy, F. W. & Von Herzen, R. P., 1971. Deep-sea corehead camera photography and piston coring, *Deep-Sea Res.*, **18**, 361–363.

McKenzie, D. P. & Sclater, J. G., 1969. Heat flow in the eastern Pacific and sea floor spreading, *Bull Volcanologique*, **33**, 101–118.

Menard, H. W., 1960. The East Pacific Rise, *Science*, **132**, 1737–1746.

Menard, H. W., Chase, T. E. & Smith, S. M., 1964. Galapagos Rise in the southeastern Pacific, *Deep-Sea Res.*, **11**, 233–242.

Menard, H. W., 1964. *Marine Geology of the Pacific*, McGraw-Hill, Inc., New York, 271 pp.

Menard, H. W., 1966. Fracture zones and offsets of the East Pacific Rise, *J. geophys. Res.*, **71**, 682–685.

Molnar, P. & Sykes, L. R., 1969. Tectonics of the Caribbean and Middle America regions, Focal Mechanisms and Seismicity, *Geol. Soc. Am. Bull.*, **80**, 1639–1684.

Morgan, W. J., 1968. Rises, trenches, great faults, and crustal blocks, *J. geophys. Res.*, **73**, 1959–1982.

Raff, A. D., 1968. Sea-floor spreading—another rift, *J. geophys. Res.*, **73**, 3699–3705.

Sclater, J. G. & Francheteau, J., 1970. The implications of terrestrial heat flow observations on current tectonic and geochemical models of the crust and upper mantle of the Earth, *Geophys. J. R. astr. Soc.*, **20**, 509–542.

Sclater, J. G., Mudie, J. D. & Harrison, C. G. A., 1970. Detailed geophysical studies on the Hawaiian Arch near 24° 25'N, 157° 40'W: A closely spaced suite of heat flow stations, *J. geophys. Res.*, **75**, 333–348.

Sclater, J. G., Anderson, R. N. & Bell, M. L., 1971a. The elevation of ridges and the evolution of the central Eastern Pacific, *J. geophys. Res.* **76**, Nov. 10.

Sclater, J. G., Jones, E. J. W. & Miller, S. P., 1971b. The relationship of heat flow, bottom topography and basement relief in Peake and Freen deeps, northeast Atlantic, *Tectonophysics*, **10**, 283–301.

Talwani, M., Windisch, C. C. & Langseth, M. G., Jr., 1971. Reykjanes Ridge Crest: A detailed geophysical study, *J. geophys. Res.*, **76**, 473–517.

Vacquier, V., Sclater, J. G. & Corry, C., 1967. Studies of the thermal state of the earth, the 21st paper: Heat flow, Eastern Pacific, *Bull. Earthq. Res. Inst. (Tokyo)*, **45**, 375–393.

Van Andel, Tj. H. & Komar, P., 1969. Ponded sediments of the mid-Atlantic ridge between 22° and 23°N latitude, *Geol. Soc. Am. Bull.*, **80**, 1163–1190.

Van Andel, Tj. H., Heath, G. R., Malfait, B. T., Heinrichs, D. F. & Ewing, J. I., 1971. Tectonics of the Panama Basin, Eastern Equatorial Pacific, *Geol. Soc. Am. Bull.*, in press.

Von Herzen, R. P., 1959. Heat-flow values from the southeastern Pacific, *Nature*, **183**, 882–883.

Von Herzen, R. P. & Maxwell, A. E., 1959. The measurement of thermal conductivity of deep-sea sediments by a needle-probe method, *J. geophys. Res.*, **64**, 1557–1563.

Von Herzen, R. P. & Uyeda, S., 1963. Heat flow through the eastern Pacific Ocean floor, *J. geophys. Res.*, **68**, 4219–4250.

Von Herzen, R. P., 1964. Ocean-floor heat flow measurements west of the United States and Baja California, *Mar. Geol.*, **1**, 225–239.

Von Herzen, R. P. & Lee, W. H. K., 1969. Heat Flow in Oceanic Regions, *The Earth's Crust and Upper Mantle, Geophysical Monograph* #13, ed. by P. J. Hart, *Am. geophys. Un.*, 88–95.

Wimbush, M., 1970. Temperature gradient above the deep-sea floor, *Nature*, **227**, 1041–1043.

Wimbush, M. & Munk, W., 1971. The benthic boundary layer, *The Sea, vol.* 4, *part* 1, ed. by A. E. Maxwell, Wiley-Interscience, 731–758.

Appendix I

The temperature gradient apparatus on Expedition AMPHITRITE (Fig. 18) consisted of a 6·5 m core barrel with three thermistor probes attached, or a short probe constructed of angle iron with two thermistors attached. The recording instrument was contained in a pressure case which descended to the bottom with the probes. The calibrated thermistor probes were individually compared in a serial time sequence with a matched thermistor probe attached near the pressure case. Temperature gradients were computed from the thermistor comparisons with an accurate bridge circuit in the bottom compared with those in the water several tens of metres above

the bottom. A sequence of thermistor and precision resistor comparisons in the bridge circuit was recorded approximately every minute.

No measurements of absolute water temperatures were made on Expedition AMPHITRITE, although precise measurements of relative temperatures were usually obtained in the water column near the bottom. Height above bottom was monitored and recorded aboard ship with data from an acoustic pinger attached to the hoisting cable. The relative accuracy of temperatures recorded by thermistor probes in the bottom is estimated to be a few thousandths °C. Deviations of the instrument axis from the vertical of more than 15° were recorded with mercury sensing switches. Values were not listed (Table 1) of the heat flow calculated over successive intervals differed by more than 10 per cent at stations where at least three probes penetrated the bottom. In fact, only one station was not included on this basis. Except perhaps for the few stations listed at which only one probe penetrated the bottom (but to a fairly-well-determined distance, judging from the bend in the probe), we consider the heat flow values accurate within about 10 per cent.

The apparatus used for temperature-gradient measurements in AII-54 cruise was improved over that on AMPHITRITE in the following ways : (1) a coring barrel of 12 m length with up to five thermistor probes attached was utilized, (2) corehead cameras (McCoy & Von Herzen 1971) on coring stations generally gave more accurate determinations of bottom penetration and vertical deviation of the corer, (3) the short probe with three thermistor probes attached spaced at 1-m intervals allowed multiple penetrations of the bottom at most stations where this apparatus was used, (4) the recording sequence repeated each 30 s, and (5) absolute water temperatures were measured by comparison with precision resistors, with errors probably less than ± 02 °C. Also, satellite navigation equipment on the ATLANTIS cruise provided positions as much as an order of magnitude more precise than the celestial navigation techniques utilized on AMPHITRITE. The ATLANTIS cruise stations at which positions were determined by satellite fixes within 1 hour of bottom penetration are listed to the nearest tenth minute in Table 2.

In addition, a more refined analysis of sediment temperature and thermal conductivities (Appendix II) permitted a more quantitative evaluation of the probable error of each heat-flow measurement (Column Q, Table 2). The success of multiple penetration of the short probe depended in part on telemetering and display of temperature information to the ship in real time. The multiple values provided important data on local variability in gradients at such stations, as discussed below. Absolute values of heat flow may be somewhat less reliable (probably less than 10 per cent error) at short probe stations than at piston-coring stations because of assumed values of thermal conductivity due to lack of core recovery.

Appendix II

All heat-flow values for AII-54 cruise were obtained from a simple computer program designated as QFIT. This program computes values for each measurement from inputs of (1) relative temperatures, with estimated errors (B_i), vs. depth in the bottom, and (2) thermal conductivity (K) values vs. depth measured on the recovered cores, or assumed from nearby stations.

The heat flow, with errors, is calculated in two ways for each station:

(1) A thermal gradient (FM), obtained by a least-squares fit of the temperature-depth data, is combined with the average of K values to give a heat-flow value (Q).

(2) Interval thermal gradients, obtained where more than two probes have penetrated the bottom, are combined with K values over the same intervals in the cores to give interval heat flows (Q_i). The heat flow is obtained from $(\sum_n Q_i)/n$, where n is the number of intervals.

Estimated errors in heat flows are obtained from method (1) by calculating independent errors in gradient and thermal conductivity. Gradient errors are in turn composed of two parts: (a) that due to differences ($DIFF_i$) of the temperature-depth data from the best fitting gradient (FM), calculated as

$$ERR1 = \left[\sum_n (DIFF_i)^2/(n-1)\right]^{\frac{1}{2}}/FM(D_n - D_1)$$

where n = number of temperature vs. depth data, and (b) that due to estimated errors in the relative temperatures (E_i), calculated as

$$ERR2 = \left(\sum_n E_i\right)/FM(N-1)^2\,(D_n - D_1)$$

The total fractional gradient error is calculated as ERRM = ERR1 + ERR2.

The average K is computed as

$$K_{avg} = \left[\sum_m \frac{1}{(1/K_i)}\right]/m$$

where m is the number of K measurements. The fractional error in K is given as

$$FSDK = \left[\sum_m (K_i - K_{avg})^2/(m-1)\right]/K_{avg} + 0{\cdot}02$$

The first part of FSDK is the usual fractional standard deviation of the measured values, and the 0·02 is added to include possible systematic errors of the needle-probe method (Von Herzen & Maxwell 1959). The error in heat flow is simply calculated as $(ERRM^2 + FSDK^2)^{\frac{1}{2}} \times Q$.

Interval heat-flow fractional errors (ΔQ_i) are computed the same way, utilizing of course only the K values of depths corresponding to the depths of each interval gradient calculation. From the several Q_i and ΔQ_i vs. depth obtained by this method, the overall Q is calculated as an average of the Q_i, and its error calculated in a way analogous to that used for the temperature gradient in method (1):

$$\Delta Q = \left[\sum_l (Q_i - Q)^2/l - 1)\right]^{\frac{1}{2}} + \frac{\left\{\sum_l \Delta Q_i\right\}}{l(l-1)} \times Q.$$

The Q of Table 2 is selected from whichever of method (1) or (2) gives the least error. Due to the nature of the data, this is usually method (1) because the estimated temperature errors (E_i) usually produce relatively large ΔQ_i by the interval method (2). However, the interval method is appropriate where the gradient and K vary inversely and significantly with depth, and those stations of AII-54 cruise by which this method results in a smaller estimated error are denoted by an asterisk in Table 2.